NASA CR-668

NASA CONTRACTOR
REPORT

NASA CR 6

# FM MODULATION
# OF A CW LASER BEAM

*Prepared by*
AIRCRAFT ARMAMENTS, INC.
Cockeysville, Md.
*for Goddard Space Flight Center*

NATIONAL AERONAUTICS AND SPACE ADMINISTRATION • WASHINGTON, D. C. • FEBRUARY 1967

NASA CR-668

# FM MODULATION OF A CW LASER BEAM

Distribution of this report is provided in the interest of information exchange. Responsibility for the contents resides in the author or organization that prepared it.

ABSTRACT

This report documents the analytical and experimental studies performed under Contract NAS5-9650. Frequency modulation and demodulation methods for CW lasers are analyzed in terms of amplitude noise sensitivity. Expressions are derived for detector noise limited signal to noise performance. Results of experiments performed with homodyne, optical discriminator and heterodyne detection breadboards are reported. An experimental transmitted reference heterodyne detection, angle modulated system is described. The modulator utilizes a 45 degree Y cut ADP crystal with length to thickness ratio of 8. Performance of the experimental breadboard over a 300 meter turbulent atmospheric path indicates that the angle modulated transmitted reference heterodyne system is insensitive to atmospherically induced noise fluctuations. Improvements in laser frequency stability are indicated to permit evaluation of broadband modulation capability.

## Table of Contents

# List of Illustrations

# I. ANALYTICAL STUDY

## A. Modulation of an Optical Carrier

An objective of this study is to investigate electro-optic methods for angle modulation of a CW laser beam. In order to present a uniform discussion of techniques implemented during the contract, introductory sections on modulation theory follow.

### 1. Phase Modulation

Consider a time dependent carrier signal of the form:

$$e(t) = E \cos (2 \pi f_c t + \theta) \qquad (1)$$

Phase modulation of the signal involves variation in the phase angle, $\theta$, of the form:

$$\theta = - K S(t) \qquad (2)$$

The modulated signal is given by substituting (2) in (1):

$$M(t) = E \cos \left[ 2 \pi f_c t - K S(t) \right] \qquad (3)$$

If the modulation signal, $S(t)$, is normalized such that $| S(t)_{max}| = 1$; K is the modulation index. It is numerically equal to the maximum value of phase deviation from the unmodulated state.

The spectrum of $M(t)$ is obtained by expanding the cosine argument and substituting the series expansions for $\cos KS(t)$ and $\sin KS(t)$.

$$M(t) = E \left[\cos (2 \pi f_c t) \cos KS(t) + \sin (2\pi f_c t) \sin KS(t)\right] \qquad (4a)$$

1

**Expanding:**

$$M(t) = E \cos (2 \pi f_c t) + E KS(t) \sin (2 \pi f_c t) \qquad (4b)$$

$$- \frac{E K^2 S^2(t)}{2!} \cos (2 \pi f_c t) - \frac{E K^3 S^3(t)}{3!} \sin (2\pi f_c t)$$

$$+ \ldots$$

If $K < < 1$, the spectrum is represented by the first two terms. This modulation is linear. Let the modulation be of the form:

$$S(t) = \cos (2 \pi f_m t) \qquad (5)$$

Substituting (5) in (4) for $K < < 1$ and expanding using the relation,

$$\sin A \cos B = 1/2 (A + B) + 1/2 \sin (A - B),$$

gives:

$$M(t) = E \cos (2 \pi f_c t)$$

$$+ \frac{EK}{2} \left[ \sin 2 \pi (f_c + f_m) t \right] + \frac{EK}{2} \left[ \sin 2 \pi (f_c - f_m) t \right] \qquad (6)$$

The phase modulated wave for small K consists of the carrier plus upper and lower sidebands in phase quadrature spaced $2 f_m$ apart. Sideband amplitude is reduced by K/2. For large values of K the spectrum becomes more complex containing integer harmonics, $f_c \pm 2 f_m$, $f_c \pm 3 f_m$, etc.

### 2. Frequency Modulation

A frequency modulated wave is described by the expression:

$$M(t) \quad E \cos \left[ 2 \pi f_c t - 2 \pi D \int S(t) \, dt \right] \qquad (7)$$

where S(t) is the modulating wave. If S(t) is normalized such that

2

$|S(t)_{max}| = 1$, the frequency deviation, $D$, is numerically equal to the maximum deviation of the instantaneous frequency from the unmodulated value, $f_c$. Define quantities as follows:

$$I_m = \left| \int S(t) \, dt \right|_{max} \tag{8b}$$

$$R(t) = \frac{1}{I_m} \int S(t) \, dt \tag{8b}$$

$$K = 2 \pi D I_m \tag{8c}$$

Substitution of these quantities permits writing (7) in the form:

$$M(t) = E \cos \left[ 2 \pi f_c t - KR(t) \right] \tag{9}$$

which is identical to a phase modulated wave where $K$ is the modulation index and $R(t)$ is the modulating signal. The spectrum of a frequency modulated wave is therefore identical to that of a phase modulated wave. Consider a modulating signal of the form

$$S(t) = \sin 2 \pi f_m t \tag{10}$$

Evaluating terms,

$$\int S(t) \, dt = \frac{1}{2 \pi f_m} \cos (2 \pi f_m t)$$

so that: $\quad I_m = \dfrac{1}{2 \pi f_m} \quad K = \dfrac{D}{f_m}$

The equivalent phase modulated wave is

$$M(t) = E \cos \left[ 2 \pi f_c t - \frac{D}{f_m} \cos (2 \pi f_m t) \right] \tag{11}$$

3

Bandwidth of the frequency modulated wave is

$$B = 2 f_m (K + 1) = 2 (D + f_m) \tag{12}$$

Wideband FM is defined by $D >> f_m$ such that $B = 2D$; narrow band FM by $D << f_m$ such that $B = 2 f_m$. Note that in the second case the bandwidth is identical to the phase modulated case where $K << 1$.

The preceding discussion of phase and frequency modulation shows that they are mathematically equivalent. In the case of modulation of a CW laser, as studied during this contract, the modulating wave is phase modulated on the optical carrier and demodulated by a frequency discriminator. It is necessary therefore to compensate the system by forming the product of the time integral of the demodulated waveform times, $2 \pi D$.

$$K R (t) = 2 \pi D \int S(t) \, dt \tag{13}$$

In this manner, frequency modulation of the CW laser beam is achieved.

3.  Transverse Pockels Effect

The method employed for modulation of the optical carrier is the transverse Pockels effect in a suitable electro-optic crystal. The voltage induced birefringence in a crystal of ordinary index of refraction, $n_o$, and extraordinary index of refraction, $n_c$, is given by

$$b = n_o - n_e = \frac{r_{a,b} \, V \, n_o^3}{t} \tag{14}$$

where:

$\frac{V}{t}$ is the applied field

$r_{a,b}$ is the eledtro-optic constant for the propagation plane in the crystal

The instantaneous phase deviation between mutually orthogonal vectors of wavelength $\lambda_c$, after propagating a distance L along the extraordinary and ordinary ray axes respectively is:

$$\Delta \phi_i = \frac{2\pi}{\lambda_c} b L \tag{15}$$

Substituting (14) for b:

$$\Delta \phi_i = \frac{2\pi}{\lambda_c} r_{a,b} V n_o^3 \frac{L}{t} \tag{16}$$

Notice that the instantaneous phase deviation is proportional to the applied voltage and the length to thickness ratio of the crystal. The practical advantage of transverse Pockels effect modulation is the reduction in required drive voltage for a fixed phase deviation associated with increased modulator crystal length.

A transverse Pockels effect modulator is shown in figure 1. Since one-half of the total retardation is attributed to each axis, i.e. the fast axis advances the wave by $\frac{\phi}{2}$ while the slow axis retards the wave by $\frac{\phi}{2}$ : and since propagation is along a single axis as shown in the figure; the expression for the modulated wave is:

$$M(t) = E \cos \left[ 2 \pi f_c t - \frac{\pi}{\lambda_c} r_{a,b} n_o^3 \frac{L}{t} V \cos (2 \pi f_m t) \right] \tag{17}$$

5
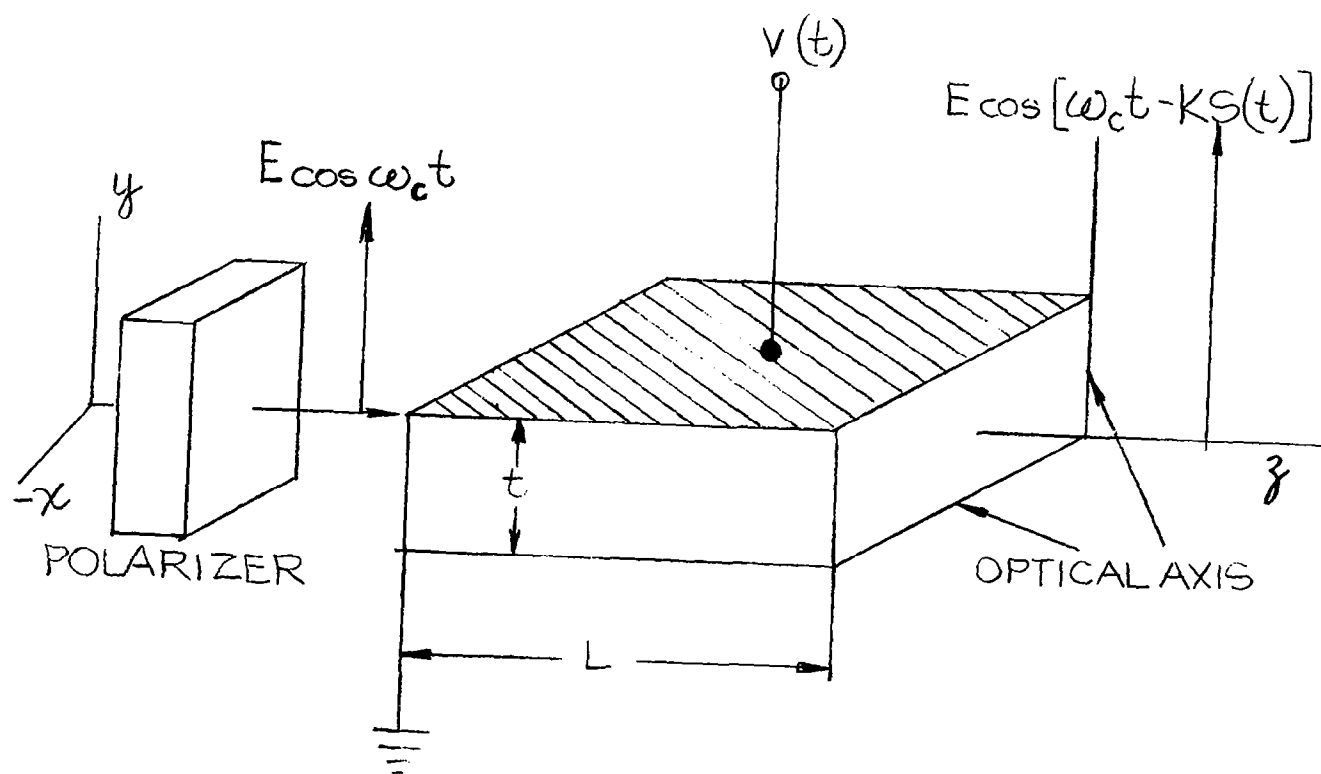
Figure 1.   TRANSVERSE POCKELS EFFECT MODULATOR

This is a phase modulated wave with:

$$K = \frac{D}{f_m} = \frac{\pi}{\lambda_c} r_{a,b} \, n_o^3 \, \frac{L}{t} \, V \; ; \quad R(t) = \cos(2\pi f_m t) \qquad (18)$$

Complexity of the spectrum of the modulated wave, or equivalently the maximum frequency deviation is determined by the modulation drive voltage on the crystal. A crystal that has a large electro-optic constant and good optical properties is desired for a transverse Pockels modulator.

B. Demodulation of an Optical Carrier

Techniques for demodulation of a frequency modulated optical carrier studied during this contract are coherent mixing, both homodyne and heterodyne; and optical discrimination, the birefringent demodulator[1] and the balanced discriminator[2]. Objective of this study is to determine the optimum demodulation scheme in terms of noise response. Specifically, this means choosing a scheme that permits limiting of the modulated wave to remove amplitude noise fluctuations while preserving the phase informa-tion. Certain advantages of FM over AM at microwave frequencies are derived from the limiting operation that makes the receiver insensitive to amplitude noise fluctuations. A system that provides similar per-formance at optical frequencies is the objective of this study. The evaluation of demodulation methods is based upon this objective.

1. Harris, S.E., "Demodulation of Phase Modulated Light Using Birefringent Crystals," Proc. IEEE, Vol. 52, No.7, pp.823-831.

2. Kaminow, I.P., "Balanced Optical Discriminator", Applied Optics, Vol. 3, Nr. 4, pp.507-510.

## 1. Homodyne Detection

Homodyne detection is a special case of heterodyne detection in which the local oscillator is an exact replica of the carrier. It involves coherent mixing of the signal modulated carrier component with an unmodulated carrier component on a suitable square law device. A practical method for implementing homodyne detection over a duplex link is to combine the signal carrier component and the local oscillator component at the transmitter; e.g. as shown in figure 2. The composite signal is transmitted to the receiver.

$$\bar{E}_2 \cos\left[2\pi f_c t - \Theta\right] \rightarrow \qquad \text{MIRROR}$$

$$E_1 \cos\left[2\pi f_c t - KS(t)\right]$$

| LASER | → | POLARIZER | → | BEAM SPLITTER | ↔ | $\lambda/4$ PLATE | ↔ | MODU-LATOR | ↔ |

MIRROR

↓ TRANSMITTED WAVE
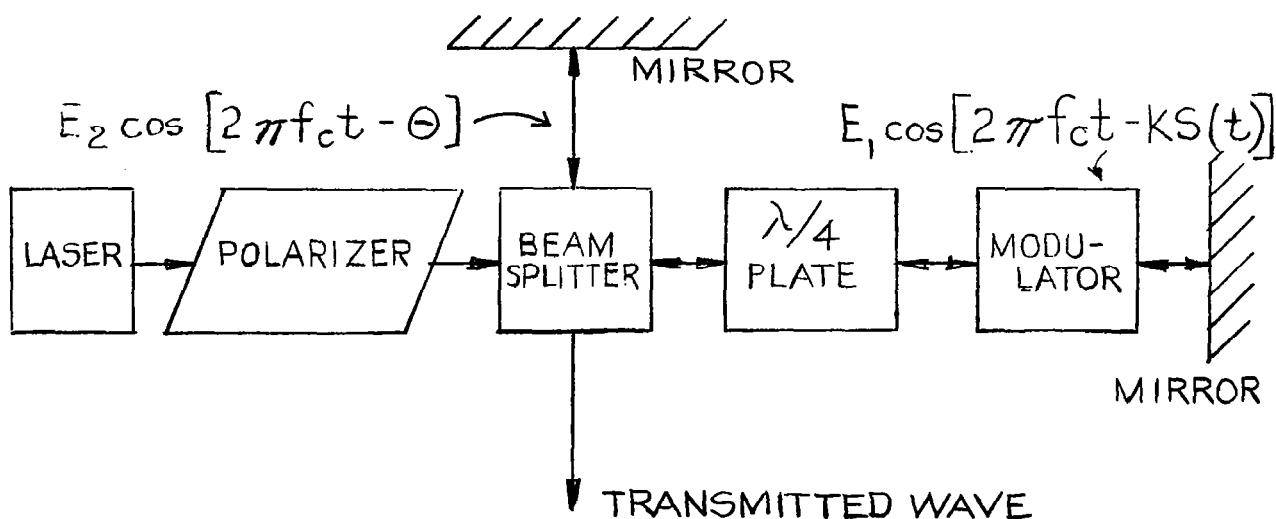
Figure 2. Optical Homodyne Transmitter

In the transmitter unit the carrier signal is intensity split into two components by an interferometer beamsplitter. One arm of the interferometer contains a double pass modulator, the other arm delays the local oscillator reference beam. The transmitted wave is described by

8

$$m(t) = E_1 \cos \left[ 2 \pi f_c t - KS(t) \right] + E_2 \cos \left[ 2 \pi f_c t - \theta \right] \quad (19)$$

where the first term is the modulated component, the second term is the reference.  Square law detection of this signal gives:

$$m^2(t) = E_1^2 \cos^2 \left[ 2 \pi f_c t - KS(t) \right] + E_2^2 \cos^2 (2 \pi f_c t - \theta) \quad (20)$$

$$+ 2 E_1 E_2 \cos \left[ 2 \pi f_c t - KS(t) \right] \cos (2 \pi f_c t - \theta)$$

The squared terms give a DC component and the second harmonic.  Using the identity $\cos A + \cos B = 2 \cos 1/2 (A + B) \cos 1/2 (A-B)$ the product term may be written:

$$e(t) = E_1 E_2 \cos \left[ 4 \pi f_c t - KS(t) - \theta \right] + E_1 E_2 \cos \left[ \theta - KS(t) \right] \quad (21)$$

The second harmonic and DC components are ignored in the detection process. If the phase difference between the two waves is an odd integer number of quarter wavelengths, i.e: $\theta = \dfrac{n\pi}{2}$, $n = 1, 3, 5 \ldots$ , the difference term is

$$e'(t) = E_1 E_2 \sin KS(t) \quad (22)$$

For $K < < 1$, the modulation is recovered.

$$e''(t) \approx E_1 E_2 KS(t) \quad (23)$$

It is apparent that the homodyne system is sensitive to variations in the carrier amplitudes $E_1$ and $E_2$.  Since it is a transmitted reference scheme, atmospherically induced phase fluctuations affect both

9

components equally and are not detectable. The relative phase angle $\theta$, between the two wave components remains constant throughout the propagation path so the condition imposed upon it is satisfied at the detector. Because the homodyne system is amplitude noise sensitive, it is not considered a suitable demodulation method for the purposes of this contract.

2.  Optical Discriminator

There are two methods of implementing direct optical discrimination of the frequency modulated optical carrier. These are the birefringent demodulator and balanced discriminator referenced earlier and shown in figures 3 and 4 respectively. Analysis of both demodulation methods is identical. In each implementation the frequency modulated carrier wave is split into two components with a relative time delay inserted between them. The beams are then recombined and square law detected.

The two signal components may be described by

$$m(t) \; = \; E \cos \left[ 2 \pi f_c t - 2 \pi D \int^t S(t) \; dt \right] \qquad (24a)$$

$$m(t-\tau) \; = \; E \cos \left[ 2 \pi f_c (t -\tau) - 2 \pi D \int^{t - \tau} S(t) \; d \; t \right] \qquad (24b)$$

where $\tau$ is the relative time delay. Square law detection of the two signals yields:

$$\left[ m(t) + m (t - \tau) \right]^2 \; = \; m^2(t) + m^2 (t - \tau) + 2m (t) m (t - \tau) \qquad (25)$$
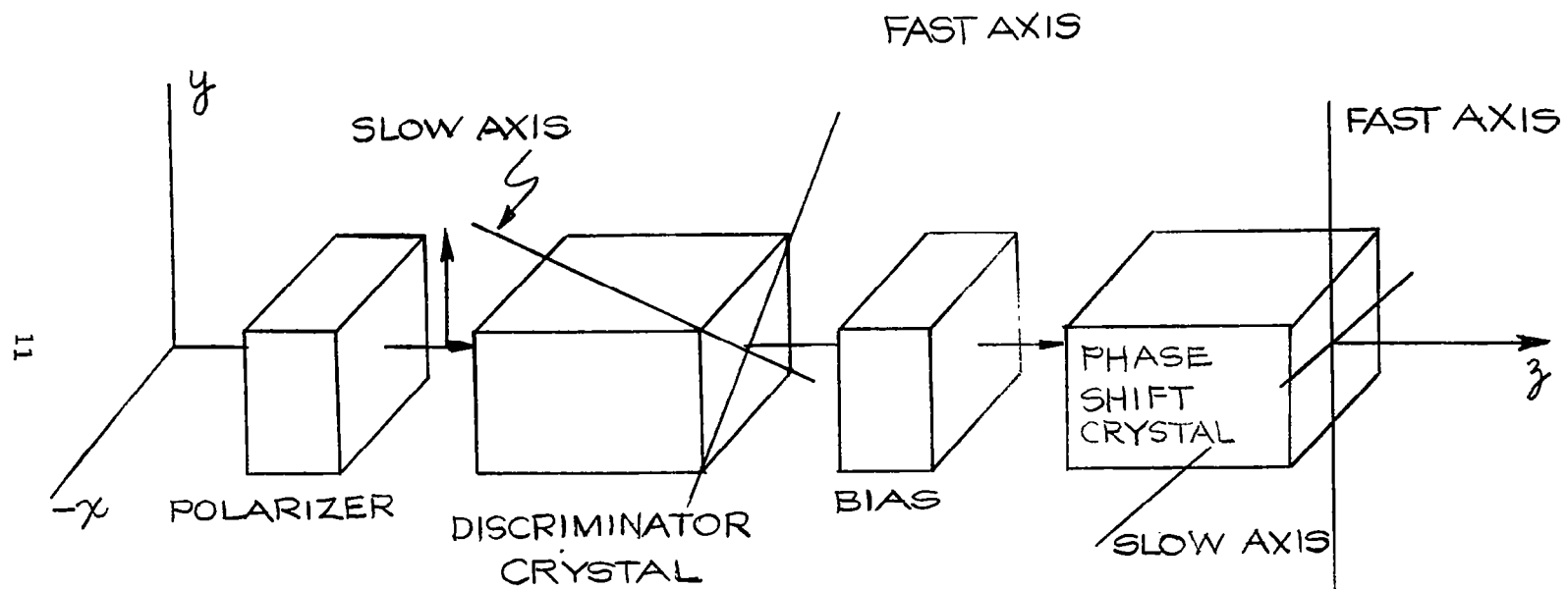
Figure 3. BIREFRINGENT FM DEMODULATOR

FAST AXIS

FAST AXIS

SLOW AXIS

POLARIZER

DISCRIMINATOR
CRYSTAL

BIAS

PHASE
SHIFT
CRYSTAL

SLOW AXIS

11

$$E\cos\left[\omega_c t - 2\pi D \int^{t} S(t)dt\right]$$

MIRROR

PHOTO
DETECTOR

BEAM
SPLITTER

$$E\cos\left[\omega_c(t-\tau) - 2\pi D \int^{t-\tau} S(t)dt\right]$$

MIRROR

MIRROR

BEAM
SPLITTER.

MIRROR
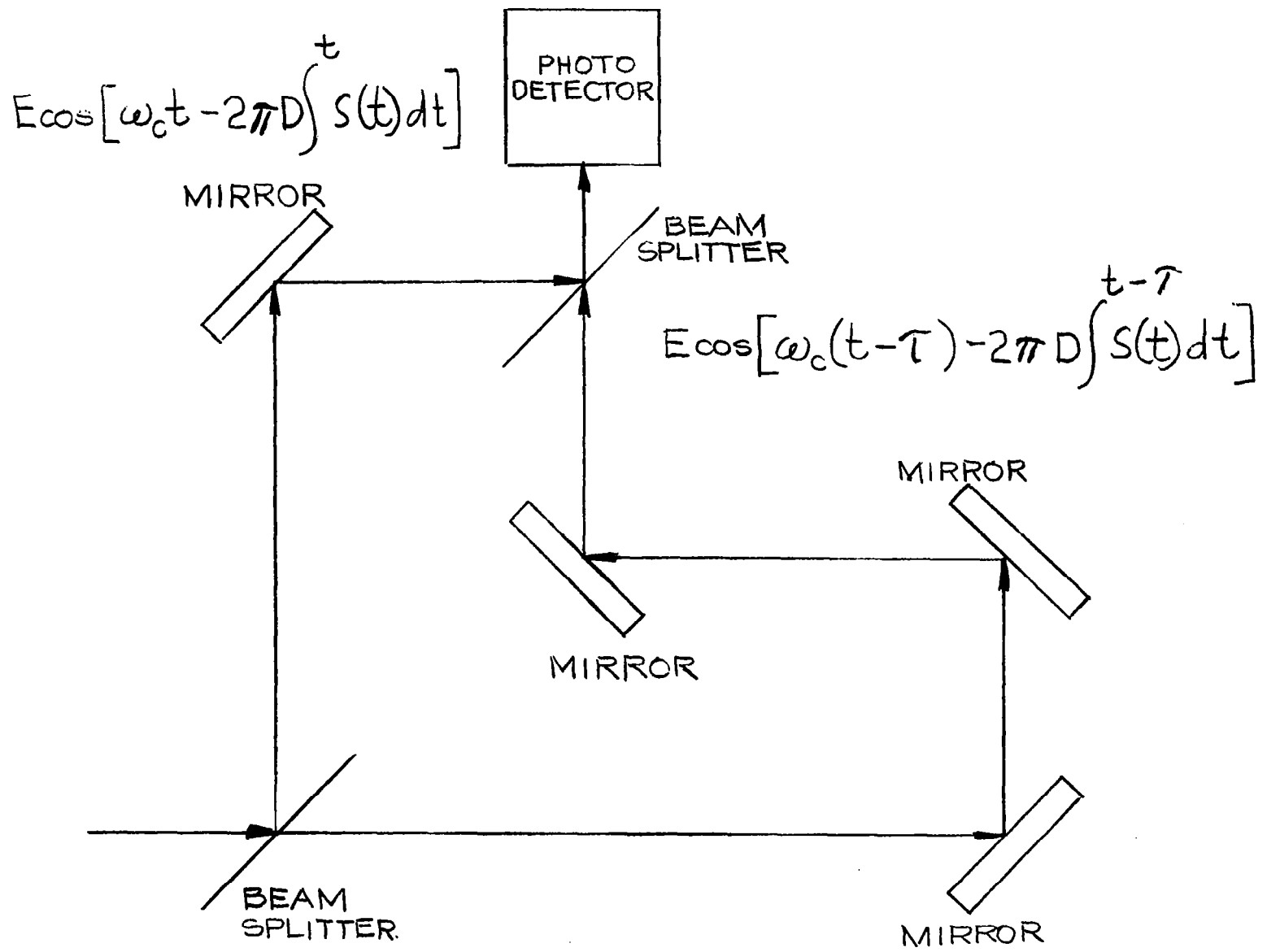
Figure 4.   BALANCED OPTICAL DISCRIMINATOR

12

Consider only the product term, that gives the sum and difference frequencies. The squared terms give DC and second harmonic components that are ignored in the detection process.

$$2\ m(t)\ m(t-\tau)\ =\ 2\ E^2 \cos\left[2\pi f_c t - 2\pi D\int^t S(t)\ dt\right]\cos\left[2\pi f_c(t-\tau)-2\pi D\int^{t-\tau} S(t)dt\right] \tag{26}$$

Using the identity, $\cos A \cos B = 1/2 \cos (A+B) + 1/2 \cos (A-B)$, and dropping the sum term, (26) may be written:

$$e(t)\ =\ E^2 \cos\left[2\pi f_c \tau - 2\pi D \int_{t-\tau}^{t} S(t)\ dt\right] \tag{27}$$

If $2\pi f_c \tau = \dfrac{N\pi}{2}$; $f_c \tau = \dfrac{N}{4}$; $N = 1,\ 3,\ 5$ then (27) becomes:

$$\left|e'(t)\right|\ =\ E^2 \sin\left[2\pi D \int_{t-\tau}^{t} S(t)\ dt\right] \tag{28}$$

Since the modulating wave, $S(t)$, is of the form $\sin \omega_m t$, the integral may be evaluated as follows:

$$\int_{t-\tau}^{t} \sin \omega_m t\ dt\ =\ -\frac{\cos \omega_m t}{\omega_m}\ +\ \frac{\cos (\omega_m t - \omega_m \tau)}{\omega_m} \tag{29}$$

Expanding $\cos (\omega_m t - \omega_m \tau)$, collecting terms, and multiplying through by $\dfrac{\tau}{\tau}$, (29) becomes:

$$\int_{t-\tau}^{t} \sin \omega_m t\ dt\ =\ \tau \sin \omega_m t \left(\frac{\sin \omega_m \tau}{\omega_m \tau}\right) - \tau \cos \omega_m t \left(\frac{1 - \cos \omega_m \tau}{\omega_m \tau}\right) \tag{30}$$

Series expansion of the terms in parentheses gives:

$$\frac{\sin \omega_m \tau}{\omega_m \tau} = 1 - \frac{(\omega_m \tau)^2}{3!} + \frac{(\omega_m \tau)^4}{5!} - \ldots \qquad (31a)$$

$$\frac{1 - \cos (\omega_m \tau)}{\omega_m \tau} = \frac{\omega_m \tau}{2!} - \frac{(\omega_m \tau)^3}{4!} + \ldots \qquad (31b)$$

For $\omega_m \tau < 2.8$ radians, where $f_m = \frac{\omega_m}{2\pi}$ is the highest frequency in S(t); an

approximation good to within 3 db is:

$$\int_{t-\tau}^{t} \sin \omega_m t \, dt \approx \tau \sin \omega_m t \qquad (32)$$

Involved here is an averaging of a sine wave over an interval $\tau$. The

constraint imposed, $\omega_m \tau < 2.8$, assures that the sine wave amplitude is

essentially constant over the averaging interval and therefore S(t) may

be removed from the integral.

With the above assumption equation (28) may be written:

$$\left| e'(t) \right| \approx E^2 \sin \left[ 2\pi \ D \ \tau \ S(t) \right] \qquad (33)$$

The sine wave is linear within 10% if $2 \pi D \tau S(t) < \frac{\pi}{4}$ or $D \tau S(t) < \frac{1}{8}$

or $D \tau < \frac{1}{8}$, since $\left| S(t) \right|_{max} = 1$. Therefore:

$$\left| e'(t) \right| \approx 2 \pi E^2 D \tau S(t) \qquad (34)$$

For sinusoidal modulation, since $K = \frac{2 \pi D}{\omega_m}$ and $D \tau < \frac{1}{8}$, then

$\omega_m \tau < \frac{\pi}{4 K}$; which is more restrictive than $\omega_m \tau < 2.8$ if $K > 0.28$.

Note that the detected signal is sensitive to amplitude fluctuations of the carrier through the dependence on $E^2$. Further, since the detector is a frequency demodulator all frequency fluctuations appear in the output through DS(t). The frequency fluctuations are proportional to the time derivative of the phase fluctuations, so phase fluctuations produce a noise output also. The system does have an amplitude noise suppression characteristic at the modulation frequency, $\omega_m$; however, this rejection falls off rapidly at either side of $\omega_m$. Comparing the optical discriminator with homodyne detection, performance is similar if $2\pi D \tau = K$

$$\text{Homodyne} \quad \left| e''(t) \right| \approx E_1 E_2 K S(t) \tag{23}$$

$$\text{Optical discriminator} \quad \left| e'(t) \right| \approx 2\pi E^2 D \tau S(t) \tag{34}$$

Since $K = \dfrac{2\pi D}{\omega_m}$, the condition for similarity of the two systems is equivalently $\omega_m \tau = 1$. Frequency and phase noise fluctuations do not affect the homodyne system however. Because the optical discriminator is amplitude noise sensitive it is not considered a suitable demodulation method for the purposes of this contract.

3.  Heterodyne Detection

A third method for demodulating a frequency modulated optical carrier is coherent heterodyne detection. This method may be implemented with the local oscillator signal generated either at the receiver or at the transmitter. In the case of a locally generated reference signal at the receiver the problem of matching phase of the two signal wavefronts

for good mixing action is a difficult task. Phase variation in the difference frequency signal generated at various points on the detector may cause total loss of signal if the wavefronts are not matched. Atmospherically induced phase distortion of the signal carrier may degrade signal performance significantly. A transmitted reference scheme for the local oscillator signal avoids the phase matching problem since both wavefronts are distorted by the intervening medium in an identical manner. If there is good mixing action at the transmitter there is good mixing anywhere in the transmitted beam.

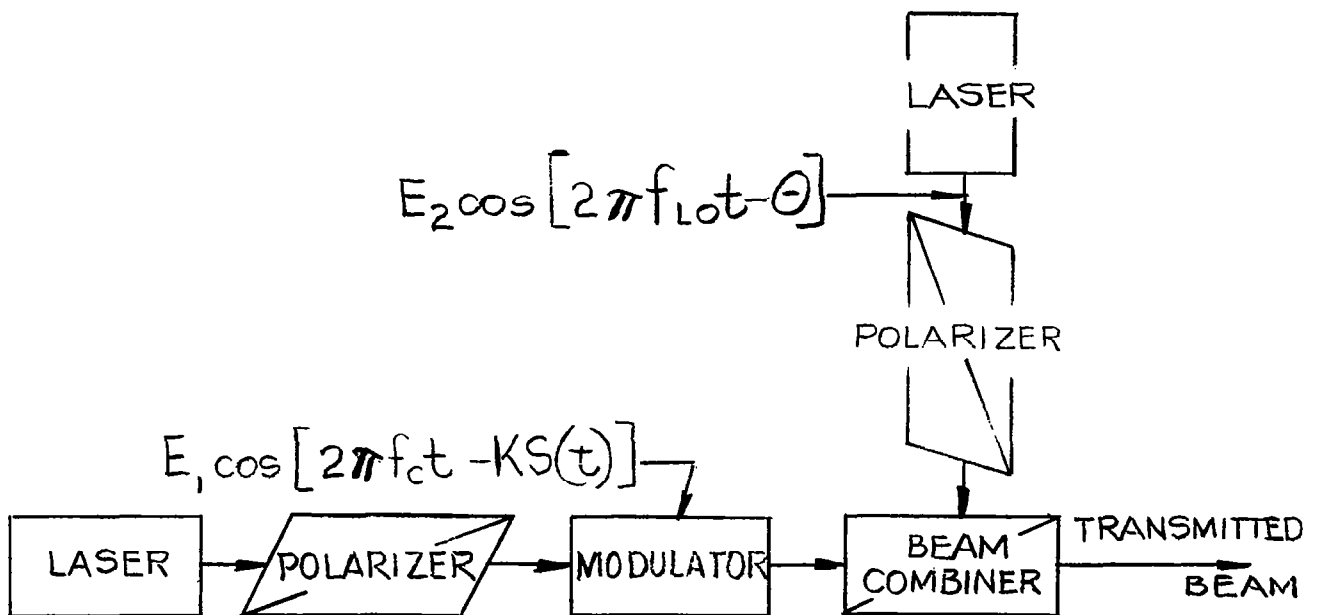A transmitted reference heterodyne system is shown in Figure 5.



Figure 5. OPTICAL TRANSMITTED REFERENCE HETERODYNE SYSTEM

The phase modulated signal carrier and frequency offset local oscillator are combined in the beamsplitter and transmitted in a collinear manner through the collimating optics. The composite waveform is described by:

$$m(t) = E_1 \cos \left[ 2 \pi f_c t - K S(t) \right] + E_2 \cos \left[ 2\pi f_{LO} t - \theta \right]$$

(35)

The first term represents a phase modulated signal carrier, the second term represents the local oscillator. Relative phase angle between the two signals is $\theta$. Square law detection of the transmitted signal consists of the familiar cosine squared terms, that give rise to a DC component and the second harmonic, and the product term that gives the sum and difference frequencies. The product term is:

$$e_o(t) = 2 E_1 E_2 \cos \left[ 2 \pi f_c t - K S(t) \right] \cos (2 \pi f_{LO} t - \theta)$$

(36)

Using the identity $\cos A \cos B = 1/2 \cos (A+B) + 1/2 \cos (A-B)$, (36) may be written:

$$e_o(t) = E_1 E_2 \cos \left[ 2 \pi (f_c + f_{LO}) t - K S(t) - \theta \right]$$

$$+ E_1 E_2 \cos \left[ 2 \pi (f_c - f_{LO}) t - K S(t) + \theta \right]$$

(37)

The second term is a phase modulated wave at the difference frequency. Since this difference frequency may be adjusted to the microwave region it may be amplified and limited to eliminate amplitude noise fluctuations and then detected. For a locally generated reference system, $\theta$ may be a complex function of the spatial coordinates on the detector photocathode.

In the case of a transmitted reference system it is a constant.

The transmitted reference heterodyne detection method is not sensitive to amplitude noise fluctuations and is unaffected by atmospherically induced phase distortion. For these reasons a transmitted reference heterodyne system is chosen for implementation on this contract. Combined with a transverse Pockels effect phase modulator, the transmitted reference heterodyne detection scheme constitutes a frequency modulated optical communications system.

C. Detector Noise Limited Performance

The desirability of implementing a transverse Pockels effect modulator and transmitted reference heterodyne demodulator to obtain an FM optical communications system is indicated in the preceding sections of this report. It is informative to investigate the signal to noise ratio at the output of the first demodulator, optical detector, for various modulation schemes. The noise power density is proportional to the average power in the signals applied to the first demodulator, which is assumed to be a square law device.

Thus:

$$N_o(f) = k P_{avg} \tag{38a}$$

and

$$\overline{n_o^2(t)} = k P_{avg} \tag{38b}$$

where $P_{avg}$ is the average power at the input to the first detector and B is the bandwidth of the demodulated wave. In the following discussion $S(t)$ or $r(t)$ represents the second modulated wave; i.e., the signal to be impressed upon the optical carrier.

1. DSSC Modulation

    In double side band suppressed carrier modulation the modulated wave may be expressed by

$$m(t) = S(t) \cos 2 \pi f_c t \qquad (39)$$

In order to demodulate this wave in a square law detector, a replica of the carrier, $E \cos 2 \pi f_c t$, must be added as shown in Figure 6.
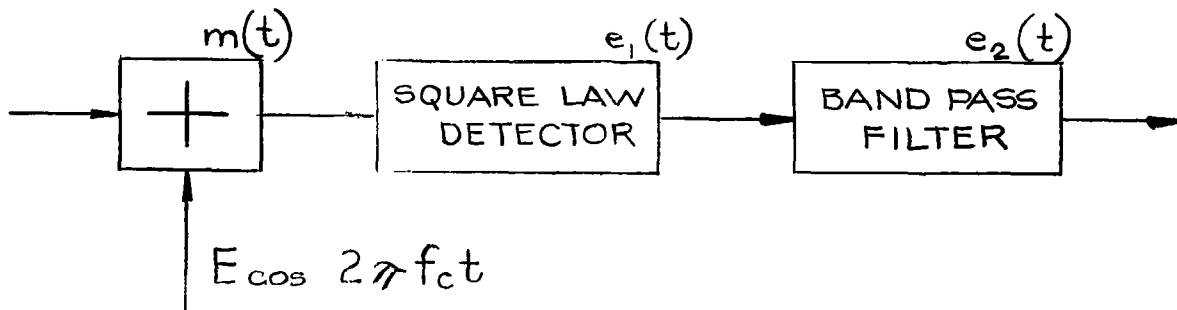


Figure 6. DSSC DEMODULATION

Output of the square law device is

$$e_1(t) = \left[ m(t) + E \cos 2 \pi f_c t \right]^2$$

$$= \left[ E + S(t) \right]^2 \cos^2 2 \pi f_c t \qquad (40)$$

by substitution of (39). Expansion of the expression in brackets and use of the identity $\cos^2 A = 1/2 + 1/2 \cos 2A$ gives:

$$e_1(t) = \left[ E^2 + 2 E S(t) + S^2(t) \right] \frac{1}{2} \left[ 1 + \cos 2 \pi (2 f_c) t \right] \qquad (41)$$

19

The output is composed of some low frequency terms, $\left[E^2 + 2\ ES(t) + S^2(t)\right]$, and some amplitude modulation of a carrier of frequency $2\ f_c$. Only the low frequency terms are passed by the bandpass filter shown in Figure 6. In addition if $S(t)$ has a bandwidth less than an octave; i.e. $f_H \leqq 2\ f_L$, where $f_H$ is the highest frequency in $S(t)$ and $f_L$ is the lowest; and since $S^2(t)$ has a D.C. term and the second harmonics of $S(t)$; then the lowest frequency in $S^2(t)$ is $2f_L$ which is greater than the highest frequency in $S(t)$ which is $f_H$. Thus $S^2(t)$ can also be separated from $S(t)$ by the bandpass filter. Output of the bandpass filter is therefore:

$$e_2(t) = E\ S(t) \tag{42}$$

Let $P_m$ equal the average power in $m(t)$ and $P_s$ equal the average power in $S(t)$. Then

$$P_m = 1/2\ P_s \tag{43}$$

and

$$\left(\frac{S}{N}\right)_{out} = \frac{E^2 P_s}{\frac{k}{2}(E^2 + P_s)B} = \frac{P_s}{\frac{k}{2}(1 + \frac{P_s}{E^2})B} \tag{44}$$

Figure 7 is a plot of $\left(\frac{S}{N}\right)_{out}$ as a function of $\frac{E^2}{P_s}$; i.e. the ratio of average carrier replica power to average power in the modulated wave. Note that $\left(\frac{S}{N}\right)_{out}$ increases as E is increased and reaches a maximum value as E approaches infinity. Not much practical improvement results, less than 1 db, if $E^2 > 4\ P_s$. Maximum signal to noise is

$$\left[\left(\frac{S}{N}\right)_{out}\right]_{max} = \frac{2\ P_s}{kB} = \frac{4\ P_m}{k\ B} \tag{45}$$
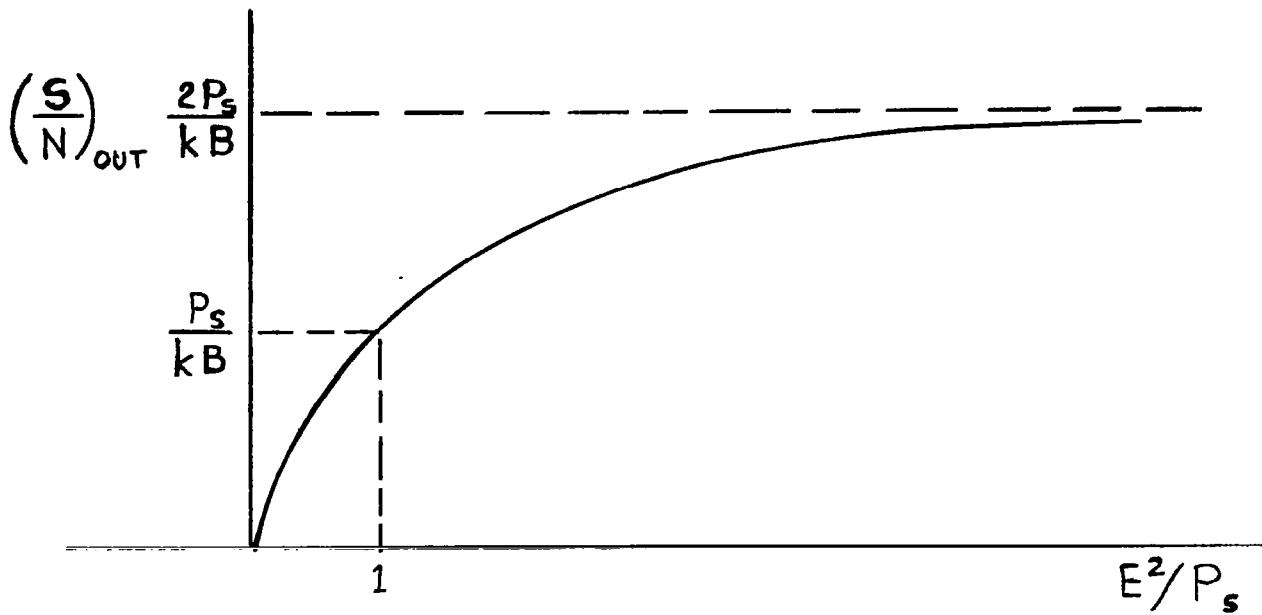
Figure 7.  SIGNAL/NOISE OUTPUT DSSC DEMODULATION

2.  Envelope Modulation

Envelope modulation is similar to DSSC modulation except that additional carrier is transmitted along with the sidebands.  The modulated wave is described by

$$m(t) \;=\; \left[ E + S(t) \right] \cos 2 \pi f_c t \tag{46}$$

This expression is identical to that for DSSC modulation at the input to the square law detector and the previous results apply with the change that the average power in the modulated wave is

$$P_m \;=\; 1/2 \; (E^2 + P_s) \tag{47}$$

Thus, (44) becomes in this case

$$\left(\frac{S}{N}\right)_{out} = \frac{E^2 P_S}{k\, P_m\, B} = \frac{(2P_m - P_S)P_S}{k\, P_m\, B} \tag{48a}$$

Simplifying

$$\left(\frac{S}{N}\right)_{out} = \frac{P_m}{k\, B}\left(2 - \frac{P_S}{P_m}\right)\frac{P_S}{P_m} \tag{48b}$$

The $\left(\frac{S}{N}\right)_{out}$ is plotted as a function of the ratio of the average signal power, $P_S$, to the average power in the modulated wave, $P_m$, in figure 8.
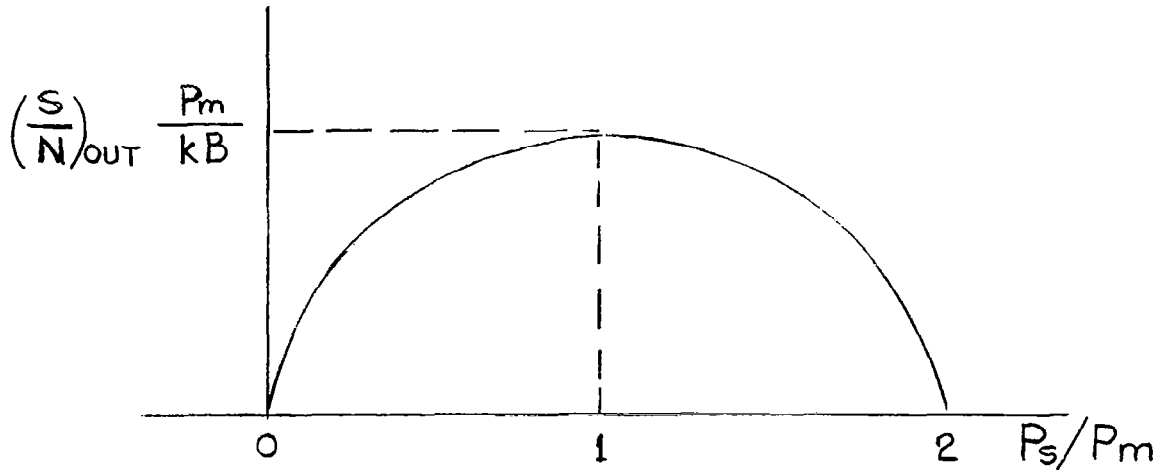


Figure 8.   SIGNAL/NOISE OUTPUT ENVELOPE DETECTION

The maximum signal to noise is

$$\left[\left(\frac{S}{N}\right)_{out}\right]_{max} = \frac{P_m}{k\, B} \tag{49}$$

22

which is less than (45), for DSSC modulation and occurs when the power in the sidebands equals the power in the carrier, i.e. $P_S = E^2$.

### 3. Phase Modulation-Heterodyne Detection

Consider a phase modulated optical carrier described by:

$$m(t) = E_1 \cos \left[ 2 \pi f_c t - KS(t) \right] \tag{50}$$

Heterodyne first detection of this signal is accomplished as shown in figure (9) by adding a local oscillator signal before the square law detector.
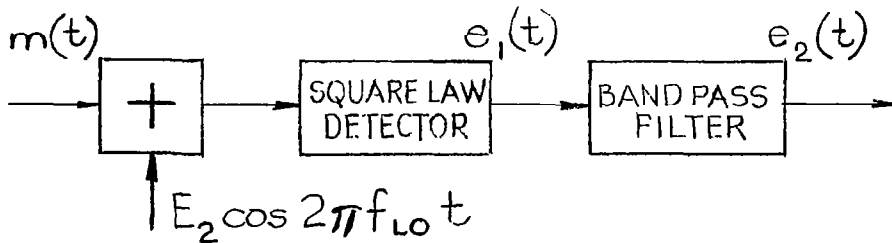


Figure 9. HETERODYNE DETECTION

Output of the square law device is:

$$e_1(t) = \left[ m(t) + E_2 \cos 2 \pi f_{LO} t \right]^2 \tag{51a}$$

$$= E_1^2 \cos^2 \left[ 2 \pi f_c t - KS(t) \right] + E_2^2 \cos^2 (2 \pi f_{LO} t)$$

$$+ 2 E_1 E_2 \cos (2 \pi f_{LO} t) \cos \left[ 2 \pi f_c t - KS(t) \right] \tag{51b}$$

Applying an argument similar to that used in the DSSC modulation case, output of the bandpass filter following the first detector is the difference frequency.

$$e_2(t) = E_1 E_2 \cos \left[ 2 \pi (f_c - f_{LO})t - KS(t) \right] \qquad (52)$$

The output signal to noise is given by the ratio of the difference frequency average power to the average noise power incident on the detector and is:

$$\left(\frac{S}{N}\right)_{out} = \frac{(E_1 E_2)^2}{k(E_2{}^2 + E_1{}^2)\,B} = \frac{E_1{}^2}{k\left(1 + \dfrac{E_1{}^2}{E_2{}^2}\right)B} \qquad (53)$$

A plot of $\left(\frac{S}{N}\right)_{out}$ versus $\left(\frac{E_2}{E_1}\right)^2$ is shown in Figure 10.
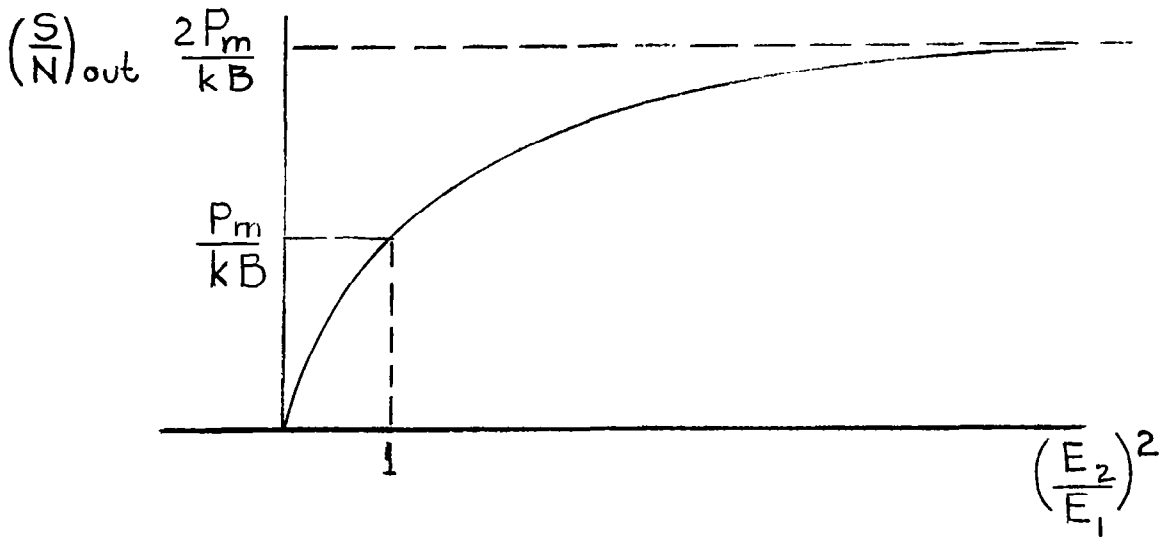


Figure 10. SIGNAL/NOISE HETERODYNE DETECTION

The maximum signal to noise is given by:

$$\left[ \left( \frac{S}{N} \right)_{out} \right]_{max} = \frac{E_1{}^2}{k \, B} = \frac{2 \, P_m}{k \, B} \qquad (54)$$

Note that this is 3 db larger than envelope modulation.

4. Angle Modulation - Optical Discriminator

Consider a frequency modulated wave of the form:

$$m(t) = A \cos \left[ 2 \, \pi \, f_c t - 2 \, \pi \, D \int^t S(t) \, dt \right] \qquad (55)$$

The average power in the modulated wave is

$$P_m = \frac{A^2}{2} \qquad (56)$$

In the optical discriminator discussed in section I.B.2., the received wave is split into two equal parts, each of amplitude E. One is delayed with respect to the other and then summed at the input to the square law device as shown in figure 11.



Figure 11. OPTICAL DISCRIMINATOR, FREQUENCY MODULATION

If the power split is equal, $E = \dfrac{A}{\sqrt{2}}$ .

Each wave component is described respectively by

$$m_1(t) = E \cos \left[ 2 \pi f_c t - 2 \pi D \int^{t} S(t) \, dt \right] \qquad (57a)$$
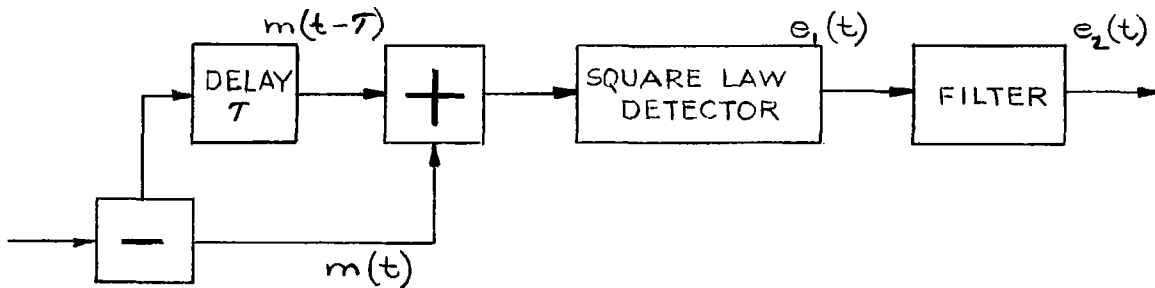
$$m_2(t) = m_1(t - \tau) = E \cos \left[ 2 \pi f_c (t - \tau) - 2 \pi D \int^{t-\tau} S(t) \, dt \right]$$
$$(57b)$$

Output of the first detector is

$$e_1(t) = \left[ m_1(t) + m_2(t) \right]^2 \qquad (58)$$

which from previous analysis, (34) is:

$$e_2(t) \approx 2 E^2 \pi D \tau S(t) = A^2 \pi D \tau S(t) \qquad (59)$$

The output signal to noise is:

$$\left( \frac{S}{N} \right)_{out} = \frac{A^4 \pi^2 D^2 \tau^2 P_s}{k B \, A^2/2} = \frac{2\pi^2 A^2 D^2 \tau^2 P_s}{k B} = (4\pi^2 D^2 \tau^2 P_s \frac{P_m}{k B} \qquad (60)$$

If $S(t) = \cos(2\pi f_m t)$ then $P_s = 1/2$ and

$$\left( \frac{S}{N} \right)_{out} = 2 \pi^2 D^2 \tau^2 \frac{P_m}{k B} = 19.6 \, D^2 \tau^2 \frac{P_m}{k B} \qquad (61)$$

As shown previously, for 10% linearity, $D \tau < 1/8$; and $D \tau < 1/4$ to make

the detector output a non-decreasing function of the input. Thus since,

$$\sin (2 \pi D \tau \cos \omega_m t) = 2 J_1 (2 \pi D \tau) \cos \omega_m t - 2 J_3 (2 \pi D \tau) \cos \omega_m t + \ldots$$

$$(62)$$

$J_1(x)$ is a maximum for $X = 1.8$ and

$$2 J_1(1.8) = 2 \times 0.582 = 1.164 \qquad \text{Thus for } D \tau = \frac{1.8}{2 \pi} = 0.286, \text{ maximum}$$

signal to noise output is

$$\left[ \left( \frac{S}{N} \right)_{out} \right]_{max} = 0.675 \frac{P_m}{k B} \qquad (63)$$

For a phase modulated wave, the analysis differs by the substitution:

$$K r (t) = 2 \pi D \int S(t) dt \qquad (64)$$

and hence, the output of the bandpass filter is

$$e_2(t) = A^2 \pi D \tau S(t) = \frac{A^2}{2} K \tau \frac{d r (t)}{dt} \qquad (65)$$

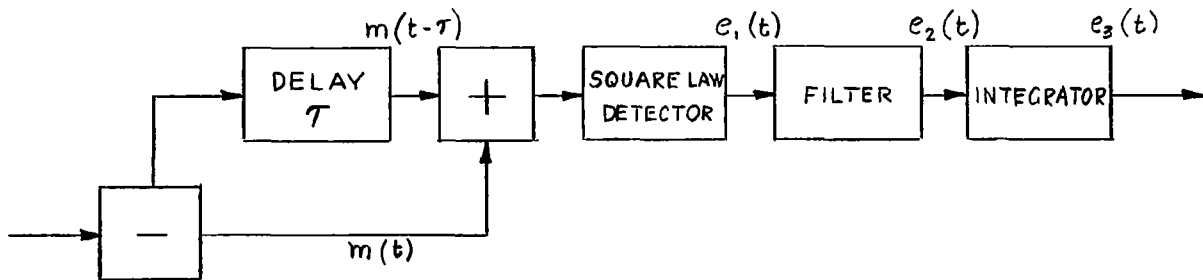Adding the integrator after the filter as shown in figure 12 gives:



Figure 12. OPTICAL DISCRIMINATOR, PHASE MODULATION

$$e_3(t) = \frac{A^2}{2} K \tau r(t) \tag{66}$$

This is the signal at the output of the integrator. The noise passes through the integrator and since $H(f) = \frac{1}{j\ 2\pi f}$, and

$$\overline{n_o^2(t)} = \int_{f_1}^{f_2} \frac{N_o(f)\ df}{(2\pi f)^2} = \frac{k\ A^2}{2\ (2\pi)^2} \int_{f_1}^{f_2} \frac{df}{f^2} \tag{67a}$$

$$= \frac{k\ A^2}{8\ \pi^2} \left[ \frac{1}{f_1} - \frac{1}{f_2} \right] = \frac{A^2\ k\ B}{8\pi^2 f_1\ f_2} \tag{67b}$$

since $B = f_2 - f_1$

The signal to noise output therefore is:

$$\left( \frac{S}{N} \right)_{out} = \frac{A^4 K^2 \tau^2 P_r}{\dfrac{4\ A^2\ k\ B}{8\pi^2\ f_1 f_2}} = \frac{2\pi^2\ A^2\ K^2\ \tau^2\ P_r\ f_1\ f_2}{k\ B} \tag{68a}$$

$$= 4\pi^2\ K^2\ \tau^2\ f_1\ f_2\ P_r\ \frac{P_m}{k\ B} \tag{68b}$$

If $r(t) = \cos \omega_m t$, $P_r = 1/2$ and the equivalent $D = K\ f_m$. In addition if $\frac{B}{f_m} << 1$; $f_1 f_2 = f_m^2$. Under these conditions

$$\left( \frac{S}{N} \right)_{out} = 2\ \pi^2\ K^2\ \tau^2\ f_m^2\ \frac{P_m}{k\ B} \tag{69}$$

For maximum $\left( \frac{S}{N} \right)$, $D\tau = 0.286 = K\ f_m\ \tau$ therefore:

$$\left[ \left( \frac{S}{N} \right)_{out} \right]_{max} = 2\ \pi^2\ (0.286)^2\ \frac{P_m}{k\ B} = 1.61\ \frac{P_m}{k\ B} \tag{70}$$

28

Summarizing the analysis presented in this section; expressions
for maximum signal to noise ratio for several modulation - demodulation
schemes considering only noise that is proportional to the average signal
power incident on the photodetector are determined. The results are
tabulated in Figure 13.

| Modulation | Demodulation | $\left[\left(\dfrac{S}{N}\right)_{out}\right]_{max}$ |
|---|---|---|
| DSSC | Homodyne | $\dfrac{4\ P_m}{k\ B}$ |
| Phase | Heterodyne | $\dfrac{2\ P_m}{k\ B}$ |
| Phase | Optical Discriminator | $\dfrac{1.61\ P_m}{k\ B}$ |
| Envelope | Direct Video | $\dfrac{P_m}{k\ B}$ |
| Frequency | Optical Discriminator | $\dfrac{0.675\ P_m}{k\ B}$ |

Figure 13.   MAXIMUM $\left(\dfrac{S}{N}\right)$ FOR SELECTED MODULATION SYSTEMS

These results indicate that considering only detector noise, of the
systems analyzed double sideband suppressed carrier modulation with
homodyne detection offers optimum signal to noise performance. It is
3 db larger than phase modulation with heterodyne detection for example.
Note however that $\left(\dfrac{S}{N}\right)$ for phase modulation with heterodyne detection
is 3 db larger than envelope modulation with direct video detection.

The $(\frac{S}{N})$ expressions are written in terms of $P_m$, the average power in the modulated wave. If a particular hardware implementation of one of the systems causes a variation in $P_m$ as compared to another approach, conclusions drawn from the relationships listed in Figure 13 do not hold. For example, transmitted reference homodyne or heterodyne schemes usually involve a 3 db loss of modulated wave signal due to the geometry of implementation. This is not common in a direct video detection scheme. It is not intended that this analysis indicate the best modulation-demodulation system for any given application. Objective of this contract is to analyze an FM optical communications system and compare it with other useful techniques. This analysis contributes to that objective.

D. Effects of Additive Noise Before Detection

The previous analysis of section I.C. treats system performance in terms of noise generated in the square law detector. Another source of noise for optical communications systems is additive background noise such as direct or reflected sunlight. Normally due to optical and spatial filtering, systems are not background noise limited. The analysis of this section treats the performance of amplitude and phase modulated systems in the presence of additive noise. The noise spectrum is described by

$$n(t) = p_n(t) \cos 2 \pi f_c t + q_n(t) \sin 2 \pi f_c t \qquad (71)$$

where $n(t)$ is bandpass, stationary, white noise of amplitude density $N_o$ and bandwidth B. Under these conditions $p_n(t)$ and $q_n(t)$ are low pass

30

white noises of amplitude density $\sqrt{2}\ N_o$ and bandwidth $\frac{B}{2}$.  Further:

$$\int_{-\infty}^{\infty} n^2(t)\ dt = \int_{-\infty}^{\omega} p_n^2(t)\ dt = \int_{-\infty}^{\infty} q_n^2(t)\ dt = \int_{-\infty}^{\infty} |N(f)|^2 df = 2\ N_o^2\ B \tag{72}$$

With these definitions the analysis proceeds.

1. Amplitude Modulation

Consider a wave amplitude modulated by a signal S(t), described as:

$$m(t)\ \ = A\ \big[\ 1 + K\ S(t)\big]\ \cos 2\ \pi\ f_c t \tag{73}$$

where $\big|\ S(t)\ \big|_{max}\ \ = \ 1$ and $K \leqq 1$.

The modulated wave plus the additive background noise is

$$m(t) + n(t) = \big[A + AKS(t) + p_n(t)\big]\ \cos 2\ \pi\ f_c t + q_n(t)\ \sin 2\ \pi\ f_c t \tag{74}$$

If this combined wave is incident upon a square law detector followed by a low pass filter, the output of the filter is:

$$e_o(t) = 1/2\ \big\{\ \big[A + AKS(t) + p_n(t)\big]^2 + q_n^2(t)\big\} \tag{75a}$$

$$e_o(t) = 1/2\ A^2 + \frac{1}{2}\ A^2 K^2 S^2(t) + \frac{1}{2}\ p_n^2(t) + \frac{1}{2}\ q_n^2(t)$$

$$+ A^2\ KS(t) + A\ p_n(t) + AKS(t)\ p_n(t) \tag{75b}$$

Assume the conditions $A >> p_n(t)$ and $K << 1$; so that:

$$e_o(t) \approx \frac{1}{2}\ A^2 + A^2\ KS(t) + A\ p_n(t) = A^2\big\{\ \frac{1}{2} + KS(t) + \frac{p_n(t)}{A}\big\} \tag{76}$$

31

The output consists under these conditions of a DC term, that is ignored, the signal, KS(t), and noise, $\underline{p_n(t)}$ .
$A$

2.  Phase Modulation

A phase modulated wave, modulated by a signal S(t) is given by

(3)
$$m(t) = A \cos \left[ 2 \pi f_c t - KS(t) \right] \qquad (3)$$

where $|S(t)_{max}| = 1$ and K is the phase deviation. The modulated signal plus the additive background noise is described by:

$$m(t) + n(t) = A \cos KS(t) \cos 2\pi f_c t + A \sin KS(t) \sin 2\pi f_c t$$
$$+ p_n(t) \cos 2 \pi f_c t + q_n(t) \sin 2 \pi f_c t \qquad (77)$$

where the expansion cos (A-B) is applied. (77) may be written in the form:

$$m(t) + n(t) = v(t) \cos \left[ 2 \pi f_c t - \theta(t) \right] \qquad (78)$$

where

$$v(t) = \left\{ \left[ A \cos KS(t) + p_n(t) \right]^2 + \left[ A \sin KS(t) + q_n(t) \right]^2 \right\}^{1/2} \qquad (79)$$

and $\quad \theta(t) = \tan^{-1} \left[ \dfrac{A \sin KS(t) + q_n(t)}{A \cos KS(t) + p_n(t)} \right] \qquad (80)$

An ideal phase detector has as its output $\theta(t)$. Since the desired signal is KS(t), the noise at the output may be described by

$$\theta_n(t) = \theta(t) - KS(t) \qquad (81)$$

Writing $\tan \theta_n(t) = \dfrac{\tan \theta(t) - \tan KS(t)}{1 + \tan \theta(t) \tan KS(t)} \qquad (82)$

which after some manipulation may be written

$$\tan \theta_n(t) = \frac{q_n(t) \cos KS(t) - p_n(t) \sin KS(t)}{A + p_n(t) \cos KS(t) + q_n(t) \sin KS(t)} \qquad (83)$$

Hence, if $A >> p_n(t)$ and $A >> q_n(t)$ and since $\cos KS(t) \leqq 1$ and $\sin KS(t) \leqq 1$

$$\tan \theta_n(t) \approx \frac{q_n(t)}{A} \cos KS(t) - \frac{p_n(t)}{A} \sin KS(t) \qquad (84)$$

and since $\tan \theta_n << 1$; $\tan \theta_n(t) \approx \theta_n(t)$

thus $\quad \theta_n(t) \approx \frac{q_n(t)}{A} \cos KS(t) - \frac{p_n(t)}{A} \sin KS(t) \qquad (85)$

Since $\cos^2 KS(t) + \sin^2 KS(t) = 1$, and since the spectrum of $q_n(t)$ is identical to the spectrum of $p_n(t)$, (both low pass, white with density $\sqrt{2} N_o$, and bandwidth $\frac{B}{2}$, it can be shown that the spectrum of $A \theta_n(t)$ is low pass, white with density $\sqrt{2} N_o$, and bandwidth $\frac{B}{2}$. Hence the output of the phase detector is:

$$\theta(t) = KS(t) + \frac{e_n(t)}{A} \qquad (86)$$

where the spectrum of $e_n(t)$ is similar to $p_n(t)$ or $q_n(t)$.

If the phase detector is not an ideal phase detector; i.e. if limiting cannot be achieved before the detector so that the output is proportional to the input amplitude; the output of the detector is given by:

$$e_d(t) = v(t) \theta(t) = v(t) KS(t) + v(t) \theta_n(t) \qquad (87)$$

33

where $v(t)$ is given by (79) which may be expanded to:

$$v(t) = \{A^2 + 2A[p_n(t)\cos KS(t) + q_n(t) \sin KS(t)] + p_n^2(t) + q_n^2(t)\}^{1/2}$$

(88)

Thus if $A >> q_n(t)$ and $A >> p_n(t)$, $v(t)$ may be written

$$v(t) \approx A\left[1 + \frac{2\,p_n(t)}{A}\cos KS(t) + \frac{2\,q_n(t)}{A}\sin KS(t)\right]^{1/2}$$

(89a)

$$\approx A\left[1 + \frac{p_n(t)}{A}\cos KS(t) \quad \frac{q_n(t)}{A}\sin KS(t)\right]$$

(89b)

This indicates that the phase detector without limiting produces noise amplitude modulation of the signal output. The degree of modulation is inversely proportional to the input signal to noise voltage ratio which is assumed to be large.

3. Comparative Evaluation

Comparing equations (86) and (76), the detector output for optimal phase modulation and amplitude modulation respectively, note that if $A >> n(t)$; i.e., if the input signal to noise ratio is large enough; both AM and PM have the same output signal to noise ratio for the same K and A. However (76) was derived under the condition that $K << 1$. If this condition is not met the output contains more noise due to the term $AKS(t) p_n(t)$ which was neglected in comparison to the term $A p_n(t)$. No restriction of this sort is placed on the derivation of equation (86). Therefore as K becomes larger, PM has an advantage over AM, in the

34

presence of additive background noise, for the same K. Obviously if a PM system can be achieved, in practice, with a larger value of K than can be achieved in an AM system, the PM system has a larger output signal to noise ratio for the same input signal to noise ratio.

II. Experimental Study

   A.  $45°$ Y Cut ADP Modulator

       1.  Electro-optic Material

           The transverse Pockels effect is chosen for the electro-optic modulator because of the dependence of the phase retardation upon the length to thickness ratio (L/t) of the crystal. As discussed in section I.A.3. the required drive voltage for a fixed ratardation is inversely proportional to the L/t ratio. A modulator with a relatively low drive voltage requirement is therefore feasible. There are a variety of electro-optic materials suitable for transverse modulators at visible wavelengths. Specifically potassium dihydrogen phosphate ($KH_2PO_4$) and its isomorphs, $KD_2PO_4$ and $NH_4 H_2PO_4$ have found widespread use in laser technology. These are class $\overline{4}2$ m crystals that have relatively large linear electro-optic coefficients. Values of $r_{41}$, which determines performance of these crystals as transverse modulators, are given in figure 14[3].

3.
    Ott, J. H. and Sliker, T. R. "Linear Electro-Optic Effects in $KH_2PO_4$ and its Isomorphs" JOSA, Vol. 54, Nr. 12, pp. 1442-1444.

| Material | Abbreviation | Electro-Optic Coefficient $r_{41}$ |
|----------|--------------|-----------------------------------|
| $KH_2PO_4$ | (KDP) | $8.77 \pm 0.14 \times 10^{-12}$ m/V |
| $NH_4H_2PO_4$ | (ADP) | $24.5 \pm 0.4 \times 10^{-12}$ m/V |
| $KD_2PO_4$ | (KDP) | $8.8 \pm 0.4 \times 10^{-12}$ m/V |

(83% - 92% deuterated)

Figure 14:  Electro-Optic Coefficient, $r_{41}$, of Selected
Class $\overline{42m}$ Materials at 546 nm.

Of these materials, ADP is the obvious choice for a transverse modulator
due to the large electro-optic coefficient.  An additional feature of ADP
is the availability of relatively large, good optical quality crystals
at low cost.  For these reasons ADP is used as the modulator material on
this contract.

2.  Modulator Configuration

A transverse modulator in ADP employs a $45^{o}Y$ cut crystal
as shown in figure 15(a).  For phase modulation of an incident linearly
polarized wave the Y axis of the crystal is oriented either parallel
or perpendicular to the polarization axis of the incident wave. The
central ray of the light beam propagates through the crystal in the XZ
plane at $45^{o}$ with respect to the Z axis.  The field is applied to the
crystal parallel to the Y axis.  Two modulator crystals were used during
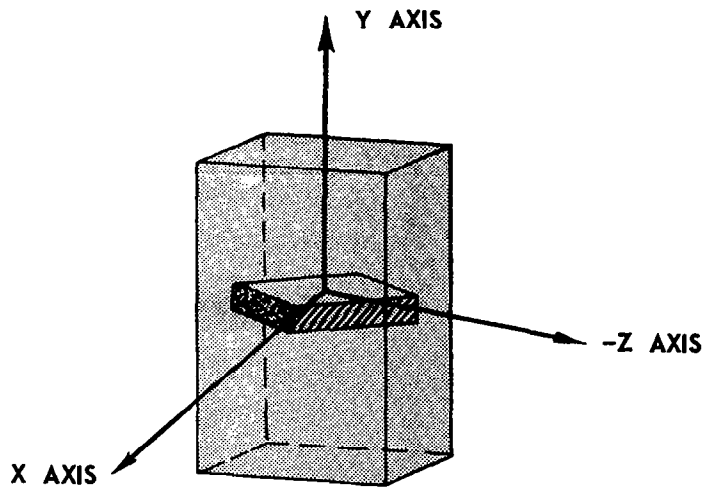the experimental work, with length to thickness ratios of 8 and 4
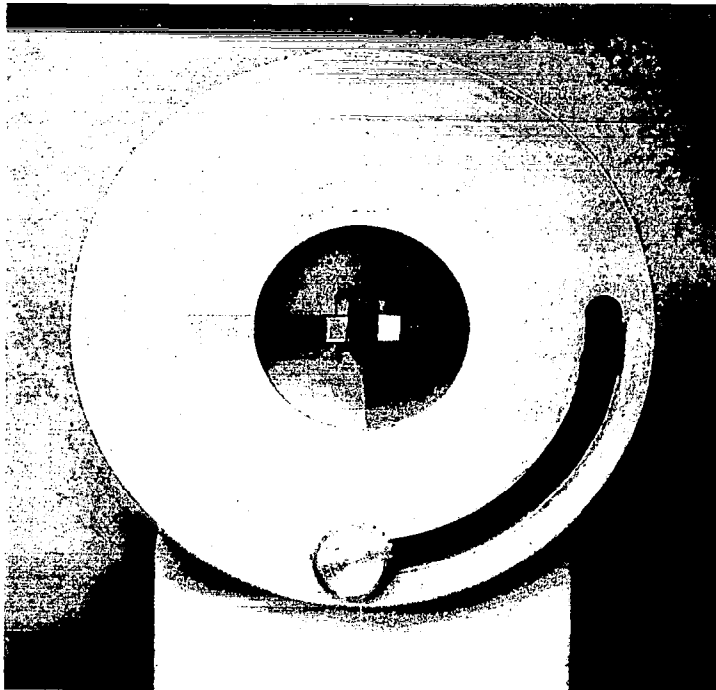
Figure 15A.  45° Y CUT ADP CRYSTAL



Figure 15B.  MODULATOR CRYSTAL HOLDER

37

respectively. The crystals are cut and polished from $45^{\circ}$ Y rod of dimensions: 3.2 mm. x 6.4 mm x 25.4 mm. Narrow dimension of the rod is along the Y axis. To prevent fogging of the polished surfaces, glass plates are applied to the end faces of the crystal with an index matching cement. The crystal is held between brass electrodes of dimensions 3.2 mm. x 6.4 mm. x 25.4 mm. that are clamped in a plastic holder (see Figure 15b.). The entire assembly is mounted in a fixture that rotates about the propagation plane of the incident light beam.

3. Modulator Performance

Performance of the $L/t = 8$ modulator was measured in a resonant circuit configuration at 50 MHz modulation frequency and in an untuned circuit at baseband, (0 - 10 MHz) modulation frequencies. The $L/t = 4$ modulator was operated only in the resonant circuit configuration.

The capacitance of the crystal and electrode structure is determined by the combination of the uniform and fringe fields. The uniform field capacitance may be calculated from the familiar parallel plate formula:

$$C_p = \epsilon_o \epsilon \frac{A}{d} \tag{90}$$

where $\epsilon_o = 8.86 \times 10^{-12}$ in mks units

$\epsilon$ = 16, dielectric constant of ADP

A = contact area of the electrodes

d = electrode separation

For the L/t = 8 crystal this is:

$$C_p = \frac{8.86 \times 10^{-12} \times 16 \times 3.2 \times 25.4 \times 10^{-6}}{3.2 \times 10^{-3}} = 3.6 \times 10^{-12} \text{ farads}$$

The fringe field capacitance is most easily determined using a graphical approximation. Flux lines and equipotentials for a half section of the crystal are shown in Figure 16. The capacitance per unit length is given by

$$C_L = \epsilon_o \epsilon \frac{N_f}{N_p} \tag{91}$$

where $N_f$ is the number of graphical flux divisions
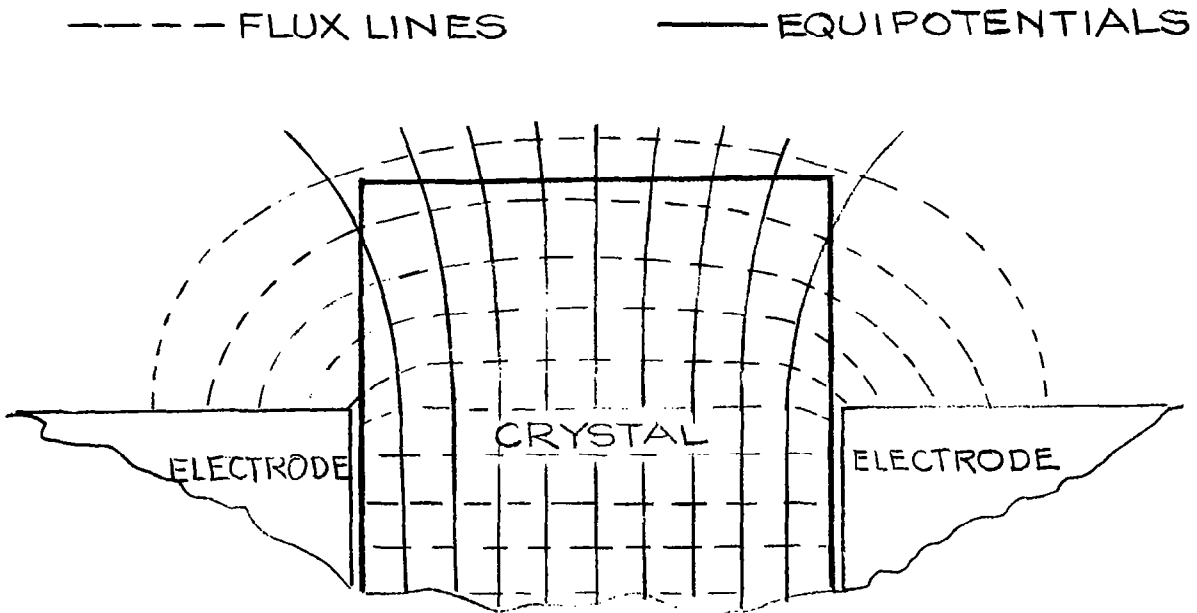
$N_p$ is the number of potential divisions.



Figure 16. GRAPHICAL ANALYSIS, FRINGE FIELD CAPACITANCE

The total fringe capacitance is $C_L$ times the crystal length.

$$C_f = 2 \times 8.86 \times 10^{-12} \times 16 \times 0.5 \times 25.4 \times 10^{-3} = 3.6 \times 10^{-12} \text{ farads}$$

Total capacitance is $\quad C_t = C_p + C_f = 7.2 \times 10^{-12}$ farads $\qquad$ (92)

This value of capacitance agrees very closely to a value determined by a bridge measurement on the crystal.

A series tuned R, L, C resonant circuit is used to impress the 50 MHz modulation carrier on the ADP crystals as shown in Figure 17.
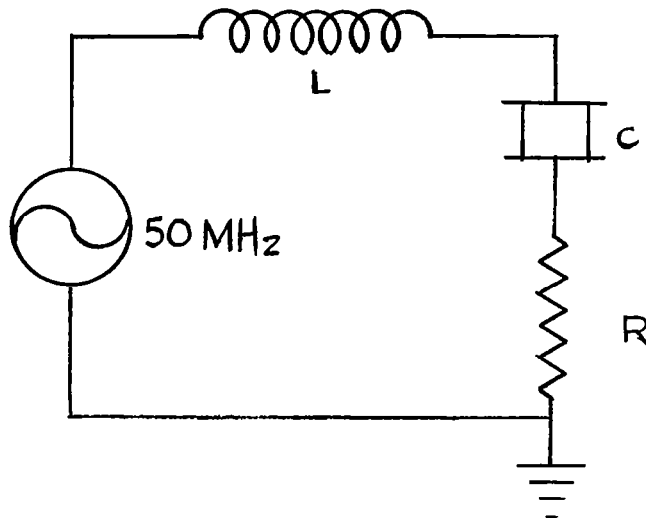
Figure 17. MODULATOR RESONANT CIRCUIT

Parameter values for the L/t = 8 crystal are: C = 7.2 x $10^{-12}$ farads, $L_i = 10^{-6}$ henries, R = 51 ohms. The resonant frequency is given by

$$f_m = \frac{1}{2\pi (L_i C)^{1/2}} = 59.4 \times 10^6 \text{ Hertz} \qquad (93)$$

The actual resonant frequency was measured at 53 MHz, due apparently to distributed capacitance in the circuit. The Q of the resonant circuit is

$$Q = \frac{2 \pi f_m L_i}{R} = 6.5 \tag{94}$$

The voltage across the crystal at the resonant frequency is

$$V_i = I X_c = \frac{E X_c}{Z} = Q E \tag{95}$$

where E is the generator terminal voltage applied to the resonant circuit, $X_c$ the reactance of the crystal, Z the circuit impedance, and I the generator current. Figure 18 is a plot of crystal voltage and resistor power dissipation as a function of generator terminal voltage for several values of circuitry Q. The generator used to test the modulator, a Johnson-Viking transmitter, has a capability of driving the circuit at 18 watts. From the chart, for a circuit Q of 6.5 the terminal voltage is 30 volts and the crystal voltage is 195 volts. Capacitance of the L/t = 4 crystal is $3.5 \times 10^{-12}$ farads. It resonates at 51 MHz with a $2.8 \times 10^{-6}$ henry inductor. Circuit Q determined by (94) is 18. For a driving power of 1 watt, voltage across the load resistor is 7.8 volts. The crystal voltage is $V = QE = 140$ volts. The high value of Q gives large crystal voltages at reduced bandwidth.

The voltage induced phase deviation in the transverse ADP modulator is given by equation (16) derived in section I.A.3.
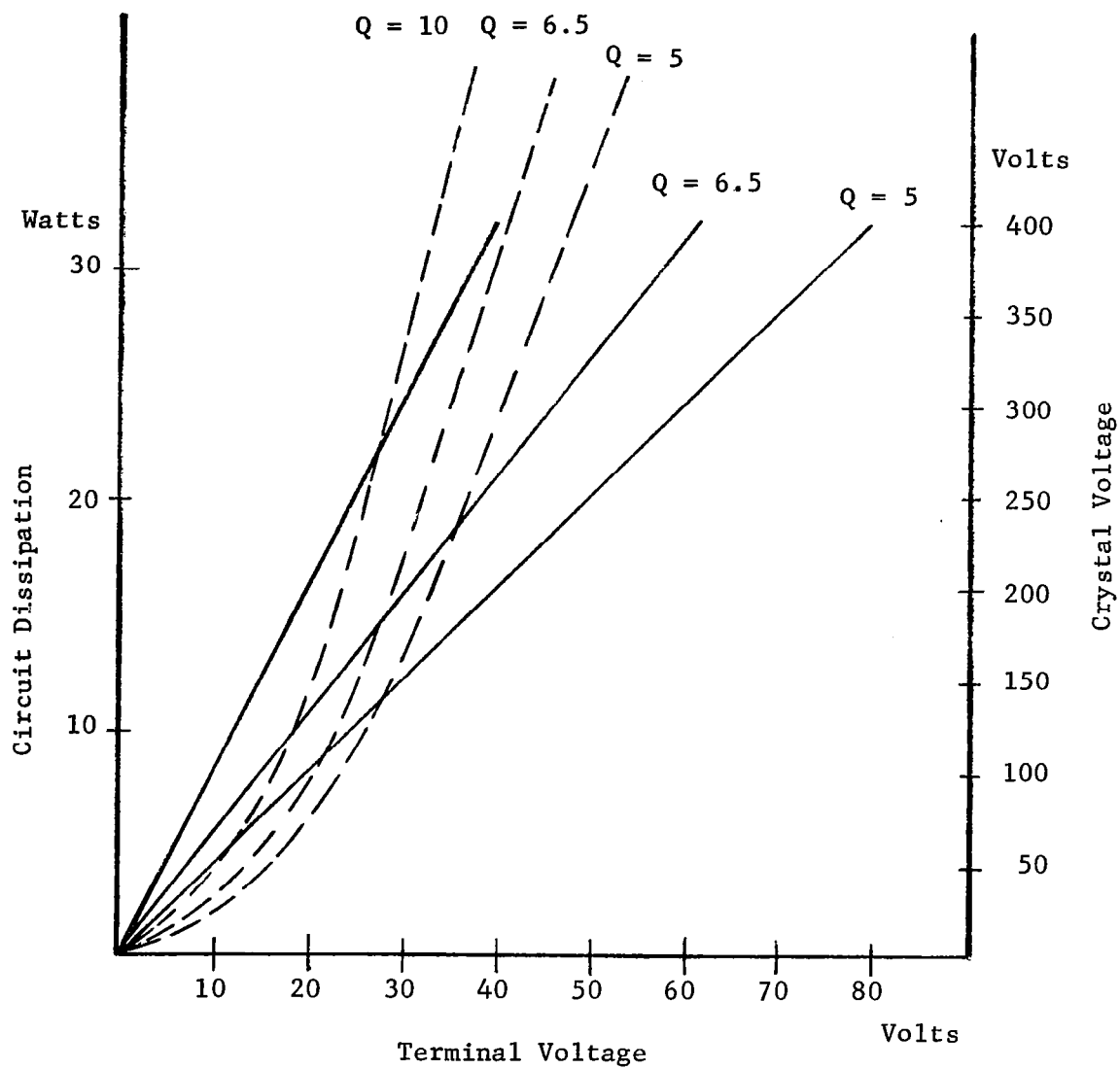
Figure 18.   CRYSTAL VOLTAGE DISSIPATION AS A FUNCTION OF
TERMINAL VOLTAGE

$$\Delta \phi_i = \frac{2\pi}{\lambda_c} r_{4,1} \, V \, n_o^3 \, \frac{L}{t} \qquad (16)$$

Value of $r_{4,1}$ at 0.546 microns is given in Figure 14. The ordinary index of refraction $n_o$ = 1.53. The phase deviation as a function of crystal voltage and $L/t$ ratio is

$$\Delta \phi = 1.01 \times 10^{-3} \, V \, \frac{L}{t} \qquad (96)$$

For $L/t$ = 8, and V = 195, $\Delta \phi$ = 1.58 radians. Maximum frequency deviation at the 53 MHz modulation frequency is

$$D = \Delta \phi \, f_m = 84 \text{ MHz} \qquad (97)$$

Evaluation of modulator performance depends upon successful demodulation. Test data for 50 MHz modulation is included in section II.B. under demodulator breadboard analysis.

Use of the ADP crystals as baseband modulators, i.e. in the frequency range 0-10 MHz; involves impressing the driving voltage directly upon the crystal as shown in Figure 19. The high gain broadband amplifier required for this application is discussed in section
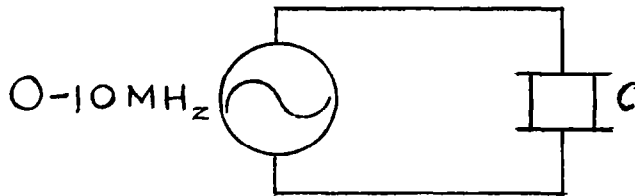


Figure 19.   BASEBAND MODULATOR

43

III. A. 3. Peak to peak drive voltages on the order of 200 volts are possible with the driver. This gives a phase deviation for the L/t = 8 crystal of 1.61 radians.

Thermal strain effects in the electro-optic crystals induce birefringence that degrades intensity modulator performance.[4] In addition to this effect, 45° Y ADP has a natural birefringence in the XZ plane that is a function of crystal rotation about the propagation axis. These effects do not degrade performance of a system that uses a demodulator that is sensitive only to instantaneous frequency deviation. Heterodyne first detection followed by an amplifier, limiter, and frequency discriminator second detector is such a system. Since the thermally induced variations or mechanical vibration about the rotation axis occur at a low frequency, typically less than 100 Hertz, even for large phase deviations of several radians the instantaneous frequency deviation is small and filterable. Experience with the two ADP mdoulators confirms this: whereas intensity modulation is severely degraded by heating of the crystal; angle modulation shows no visible effect. The crystal may be rotated several degrees about the propagation axis, also with no visible effect upon angle modulation but with deleterious effect upon intensity modulation.

[4] Kaminow, I.P. "Strain Effects in Electro-optic Light Modulators" Applied Optics Vol. 3, Nr. 4, pp. 511-515.

The preceding discussion demonstrates the usefulness of a 45° Y cut transverse ADP modulator in a variety of operational configurations. The L/t = 8 crystal is chosen as the optimum modulator for this contract due to the large phase deviation obtainable with moderate drive voltage.

B.  Demodulator Breadboards

Optical breadboards of homodyne, optical discriminator, and heterodyne demodulators were constructed and tested to experimentally verify modulator performance. The test results confirm the conclusions drawn in the analytical study portion of the program; specifically, that the homodyne and optical discriminator techniques are amplitude noise sensitive.

1.  Homodyne

Arrangement of the homodyne optical breadboard is shown in Figure 20. The interferometer assembly is mounted on 18 mm. thick aluminum surface plate for stability. The beamsplitter is a mirror type with 30% reflectance and has surfaces parallel to 20 seconds of arc. The interferometer mirrors are dielectric coated flats with maximum reflectivity at the laser wavelength and are mounted on holders with three point adjustment for ease of alignment. The reference beam mirror is mounted on a slide carriage, adjustable along the optical axis. The Pockels modulator is contained in a rotatable holder placed on the optical axis of the signal arm of the interferometer. Direction of rotation is about the
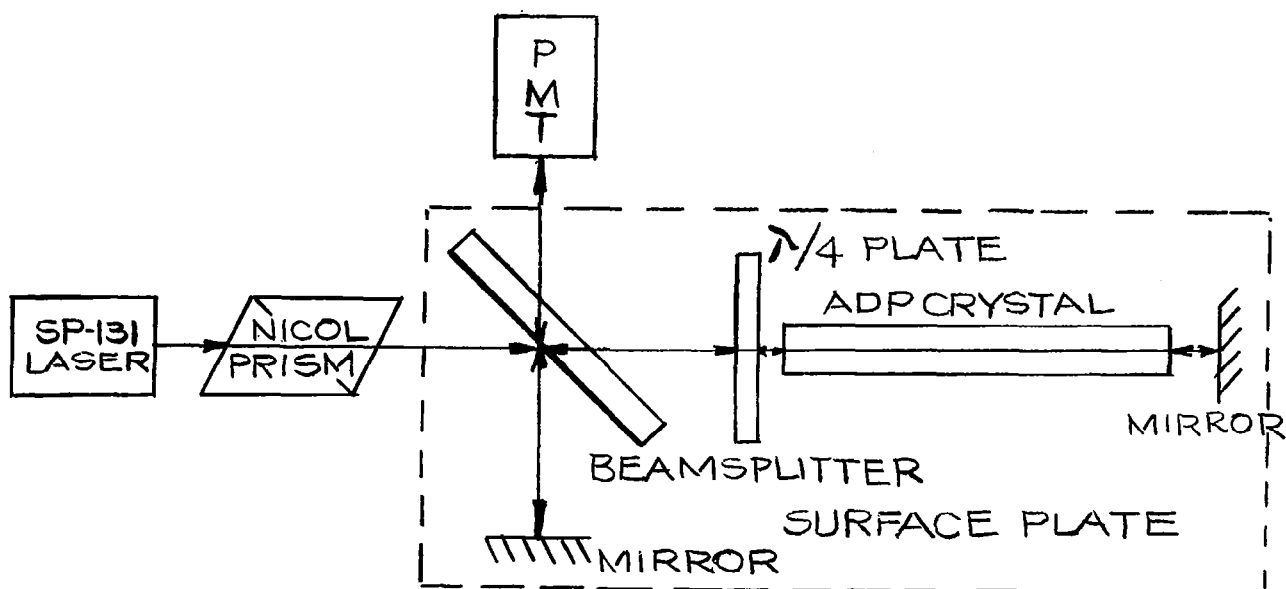
Figure 20.  HOMODYNE OPTICAL BREADBOARD

optical axis.  The laser is a Spectra Physics model 131 operated in the

hemispherical mode without external beam forming optics.  Power output

is 0.5 milliwatt and beam divergence is less than 0.7 milliradians.  The

polarizer is a Nicol prism.  The laser, polarizer, and interferometer

are rigidly mounted to a 10 cm. wide, dual rail optical bench.  The photo-

multiplier detector is an RCA experimental type C70042 CP and is mounted

on a separate stand at right angles to the optical bench.

There are several important factors involved in the opera-

tion of the homodyne demodulator.  It is essential for good mixing action

on the photodetector that the signal beam and the reference beam be

exactly parallel and superimposed.  The degree of alignment is checked

by noting the interference fringes between the two beams displayed on a white card at the detector location. Two or three wide dark fringes within the beam pattern indicate adequate spatial phasing of the two lasers. Relative time phase between the signal and reference waves is adjusted to $n\frac{\pi}{2}$, where n is a small integer. This is accomplished in one, or a combination, of three ways: angular orientation of a quarter wave retardation plate in the signal arm, angular orientation of the naturally birefringent 45 degree Y cut ADP crystal, or adjustment of the reference beam optical path length. In the breadboard model there is sufficient vibration of the mirrors to give a time average of the optimum alignment conditions.

A useful feature of the homodyne breadboard is the double pass modulator configuration. Both the 8 to 1 and 4 to 1 length to thickness ratio crystals were used in the assembled breadboard. Phase retardation for the 8 to 1 crystal at 5 watts drive is 1.84 radians; for the 4 to 1 crystal at 1 watt drive power the phase retardation is 1.12 radians. Both values of phase shift exceed the conditions for linear modulation, i.e. $K \ll 1$. For both modulators, detected signal amplitude in the breadboard system is insensitive to drive power variations due to saturation caused by the nonlinearity.

Input to the photomultiplier detector is filtered both optically and spatially to prevent current saturation. Output of the detector is fed to a UHF receiver consisting of an APR-4 receiver unit

and a 541 Tektronix oscilloscope and/or a Polarad spectrum analyzer. The demodulated sine wave and frequency spectrum for 5 watts drive power at 52 MHz on the 8 to 1 crystal are shown in Figure 21. A drift in wave amplitude is noticeable as the RF power heats the crystal. This is compensated by rotation of the crystal. Amplitude sensitivity of the homodyne system is demonstrated by inserting neutral density filters in the optical path between the interferometer and the detector.

Experience with the homodyne demodulator breadboard demonstrates: sensitivity of the system to vibration through variations in the relative optical path length difference between the two arms of the interferometer, non-linear detection for large values of phase deviation, and sensitivity of the system to amplitude fluctuations in the transmitted beam. The first item is corrected by rigid mechanical design of the interferometer. The analysis performed during the analytical study predicts non-linear detection for large values of phase deviation, K; and the amplitude sensitivity of the system as demonstrated in the experimental model.

2. Optical Discriminator

A diagram of the optical discriminator breadboard is shown in Figure 22. The interferometer assembly is mounted on 18 mm. thick aluminum surface plate for mechanical rigidity. The maximum path length difference between the two arms is 60 cm.; and it is adjusted by motion of a mirror mounted on a slide carriage assembly. Separation of the

A - 52 MHz Modulation

ADP Crystal Drive
Power - 5 Watts
L/t = 8

B - Spectrum Analyzer
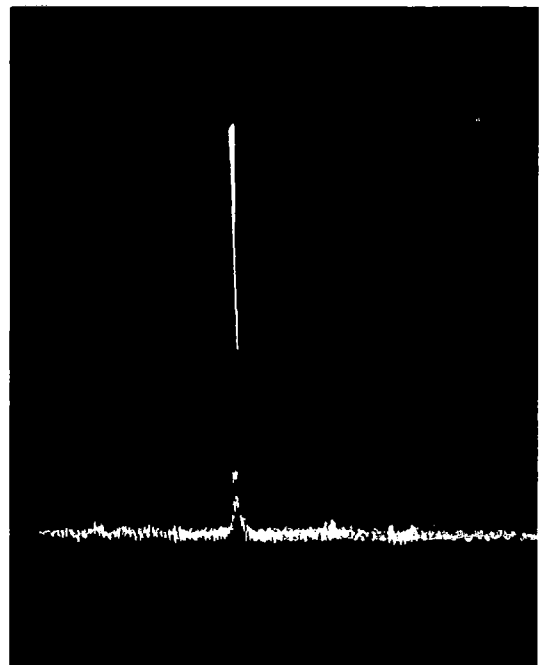
Center Frequency 50 MHz
RF Drive 5 Watts
L/t = 8



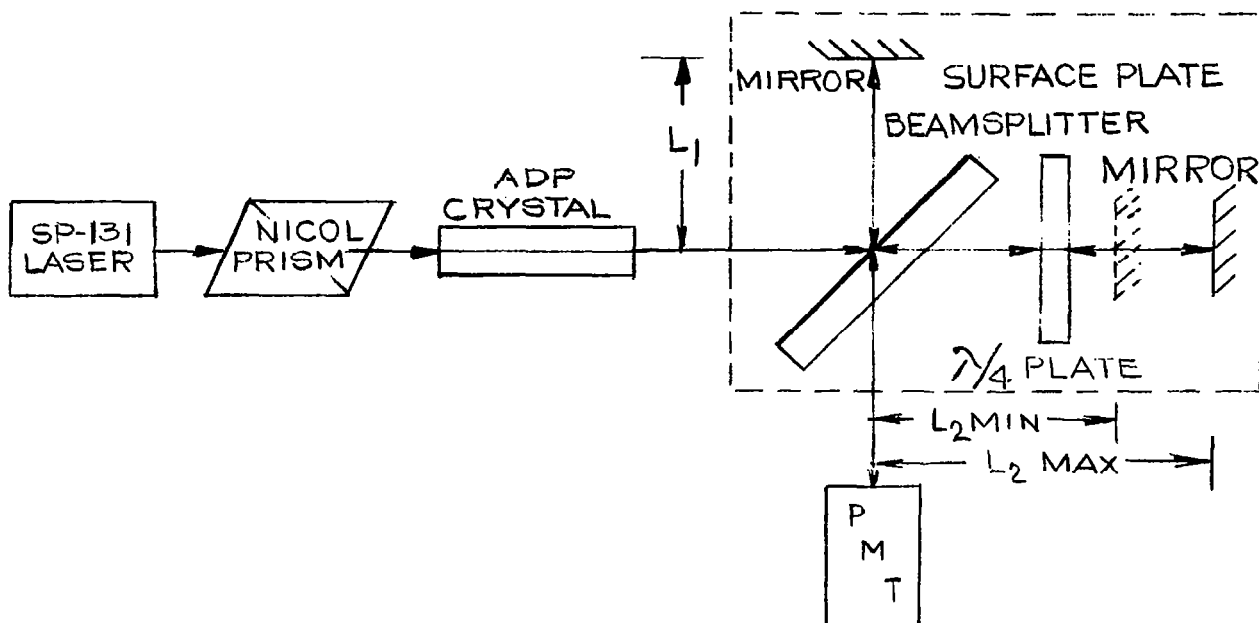Figure 21.   HOMODYNE DETECTED SIGNAL

Figure 22.  OPTICAL DISCRIMINATOR BREADBOARD

fixed mirror and the mirror beamsplitter, $L_1$ is 5 cm; separation of the movable mirror and the beamsplitter, $L_2$ (max.) = 35 cm., $L_2$ (min.) = 2 cm. The mirrors are dielectric coated flats with maximum reflectance at the laser wavelength.  They are installed in three point adjustable mounts for ease of alignment.  The mirror type beamsplitter is the same one used in the homodyne breadboard.  The laser is a Spectra-Physics model 131 operating in the hemispherical mode.  The laser, Nicol prism polarizer, modulator, and interferometer are mounted on the 10 cm. optical bench.  The photomultiplier detector, type C70042CP, is mounted on a separate stand perpendicular to the optical bench.  A quarter wave plate is placed in the adjustable length interferometer arm on a rotatable

holder.  The modulator may also be rotated about the optical axis.

Several conditions must be satisfied for satisfactory operation of the optical discriminator.  As in the case of homodyne detection the two beams must be exactly parallel and superimposed for good mixing action on the photomultiplier.  Interference fringes are observed to determine optimum spatial phasing of the two beams.  The condition $f_c \tau = \frac{n}{4}$ , (equation 27), is satisfied by rotation of the quarter wave plate.  The other condition that must be satisfied is $\omega_m \tau < 2.8$ for $K < 0.28$ or $\omega_m \tau < \frac{\pi}{4K}$ for $K > 0.28$.  Recall that these conditions are derived from the requirements for linear detection (equations 32 ff).  The value for K is given by (96),

$$K = 10^{-3} V \frac{L}{t} \tag{96}$$

The $L/t = 4$ modulator crystal is used in this work, so $K = 4 \times 10^{-3} V$. The angular frequency for 51 MHz modulation is

$$\omega_m = 2 \pi f_m = 3.2 \times 10^8 \text{ radians/sec.} \tag{98}$$

The maximum delay time, $\tau_{max}$, is:

$$\tau_{max} = 2 \left[ \frac{L_{2 \text{ (max)}} - L_1}{c} \right] = 2 \times 10^{-9} \text{ sec.} \tag{99}$$

The minimum delay time, $\tau_{min}$, is:

$$\tau_{min} = 2 \left[ \frac{L_{2(min)} - L_1}{c} \right] = 1.25 \times 10^{-9} \text{ sec.} \tag{100}$$

where c is the velocity of light, $3 \times 10^8$ meter/sec.

Therefore:

$$\left. \begin{array}{l} \omega_m \, \tau_{max} \;\; = \;\; 0.64 \;\; \text{radians} \\[20pt] \omega_m \, \tau_{min} \;\; = \;\; 0.4 \;\; \text{radians} \end{array} \right\} \tag{101}$$

In order to determine which condition on $\omega_m \tau$ applies, it is necessary to computer K for the drive voltages used. Data is taken at three input power levels: 0.5, 2, & 5 watts. Voltage across the crystal with a Q of 18 for a circuit R of 50 ohms is 90, 180, and 284 volts respectively. The corresponding K's are shown in Figure 23.

| Drive Power | Applied Voltage on Crystal | Retardation K | $\dfrac{\pi}{4\,K}$ |
|---|---|---|---|
| (a) 0.5 watts | 90 volts | 0.36 | 2.18 |
| (b) 2.0 watts | 180 volts | 0.72 | 1.09 |
| (c) 5.0 watts | 284 volts | 1.14 | 0.704 |

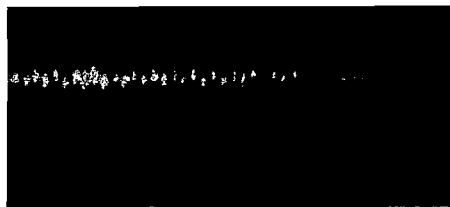Figure 23.  PARAMETERS FOR L/t = 4 Crystal in Optical Discriminator

In each case $K > 0.28$, therefore $\omega_m \, \tau < \frac{\pi}{4K}$ must apply for linear detection. In each case this condition is satisfied for all values of $\omega_m \, \tau$. Figure 24 shows the detected sine wave for 52 MHz modulation at the three values of drive power for three values of $\omega_m \, \tau$. The receiver is an APR-4 receiver unit in combination with 541 oscilloscope. The data shows a trend toward increased output amplitude proportional to drive power and $\omega_m \tau$ as predicted by the analysis, (equation 34); although comparison of specific data is
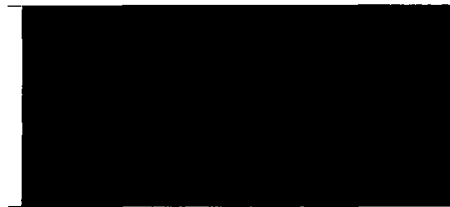
0.5 Watts
K = 0.36

2 Watts
K = 0.72

5 Watts
K = 1.14

Minimum Path Length $\omega_m \tau = 0.4$
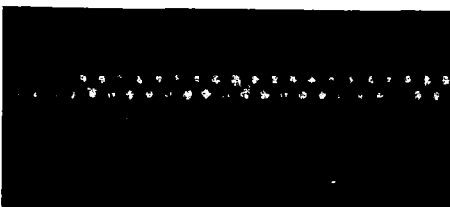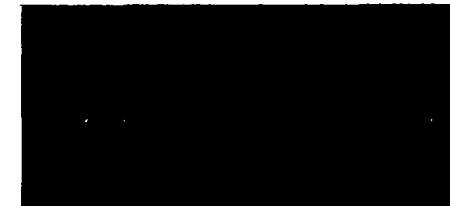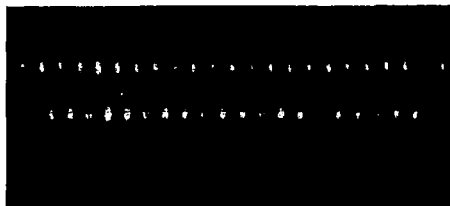
Mean Path Length $\omega_m \tau = 0.52$

Maximum Path Length $\omega_m \tau = 0.64$

Figure 24. OPTICAL DISCRIMINATOR DETECTED SIGNAL

not in agreement. This inconsistency is due to instability in the bread-board caused by mechanical vibration of the mirror mounts. Also the range of $\omega_m \tau$ is limited by the mechanical layout on the surface plate. Sensitivity of the optical discriminator to amplitude variations is observed by inserting neutral density filters in the beam between the modulator and beamsplitter. No attempt was made to observe the AM rejection at the modulation frequency, $\omega_m$.

   3. Heterodyne

   Arrangement of the optical breadboard for heterodyne detection is shown in Figure 25.
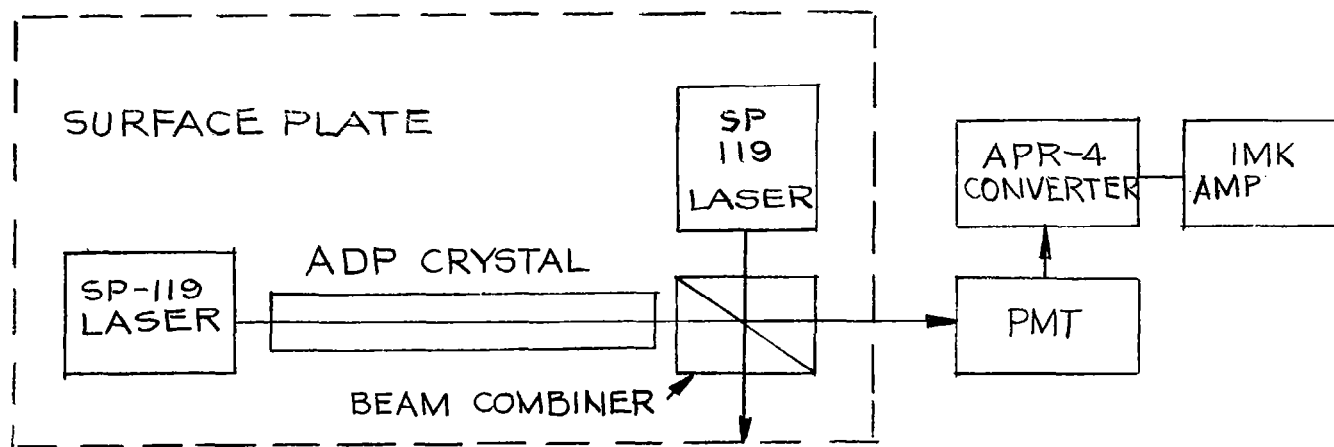
Figure 25   HETERODYNE OPTICAL BREADBOARD

   The transmitter unit consists of a signal laser, reference laser, Pockels modulator, and right angle prism beam combiner. The lasers are Spectra-Physics model 119, chosen for single mode and stable frequency operation. The temporal coherence of the output radiation is achieved by

use of a stabilized optical resonator of such short length that only a single mode can be sustained.  The plasma tube is mounted in an invar resonator structure having bi-metallic temperature compensation.  One of the dielectric resonator mirrors is mounted on a piezo-electric element which is voltage controlled for mirror spacing with resultant control of laser frequency.  A photodetector and servo controller permit locking of the mirror drive voltage to the Lamb dip region of the lasing mode.  The resonator and plasma tube are housed in a temperature controlled oven for thermal stability.  Surrounding the oven is a mu-metal cover which shields the invar resonator from magnetostrictive modulation effects caused by stray external magnetic fields.  These lasers are servo locked to a fixed offset difference frequency of 200-300 MHz.  The phase modulation on the signal carrier is transferred to the difference frequency  upon square law detection of the two signals at the receiver.

The breadboard receiver unit consists of a C70042CP photo-multiplier detector, APR-4 tuning unit modified to a 60 MHz intermediate frequency, and a LEL model IMK amplifier, limiter, discriminator unit. The phase modulated difference frequency is converted down to the intermediate frequency of the FM receiver unit and subsequently detected. In this experimental work a subcarrier modulation in the range 0-2 MHz is used in order to stay within the 3 db bandwidth of the receiver units. Successful results obtained with the experimental model i.e. mixing of the two laser frequencies to obtain the difference frequency, and detec-tion of subcarrier modulation, led to an early decision to implement this

heterodyne detection method in the experimental breadboard. Detailed

discussion therefore of the experimental data is included in following

sections of this report.

III. BREADBOARD SYSTEM

A. Hardware Description

A block diagram of the transmitted reference heterodyne laser

communications system is shown in Figure 26. There are three basic

elements of the system: the transmitter unit, the receiver unit, and the

modulation-demodulation electronics. Shown in the diagram is the implemen-

tation for single frequency subcarrier modulation. Operation of the system

is identical to that of the experimental system described in section II.B.3.

1. Transmitter Unit

Photographic views of the transmitter unit are shown in

Figure 27. Picture A is an exterior view showing the unit cover, colli-

mating telescope, and 7X spotting scope. Picture B is an interior view

showing the arrangement of the optical components: lasers, modulators,

beam combiner, and eyelens of the collimating telescope. Picture C shows

the transmitter unit mounted on the tripod at one of the experimental test

sites. The laser power supplies with integral servo controllers are placed

on the tripod base plate. The tripod is adjustable 360 degrees in azimuth

and approximately 30 degrees in elevation. Picture D shows the detail of

the mounting adjustment for the lasers.

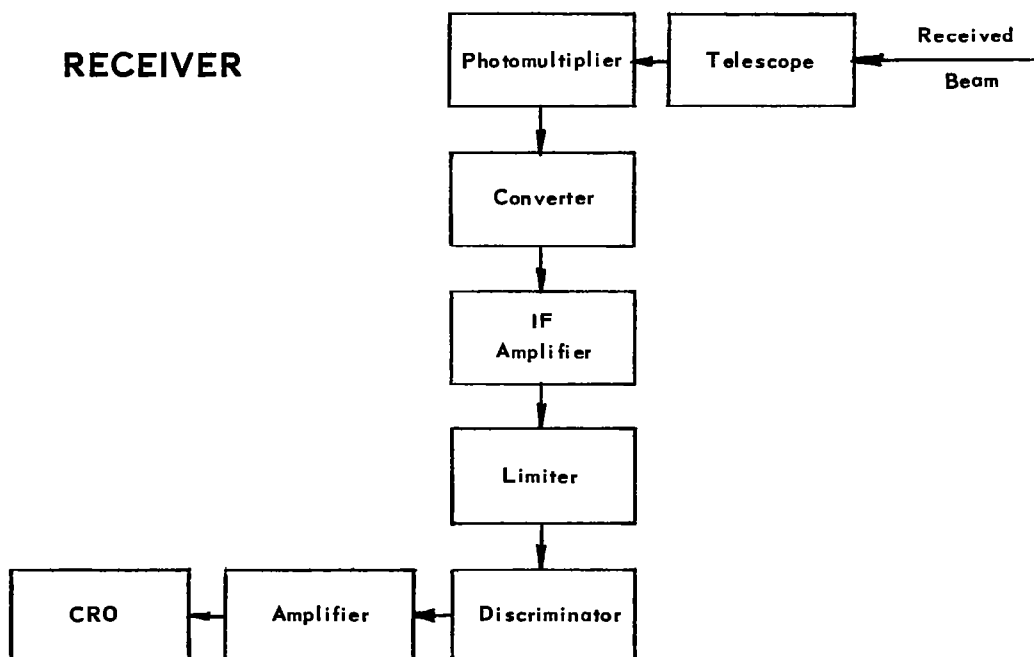The baseplate for the transmitter unit is fabricated from
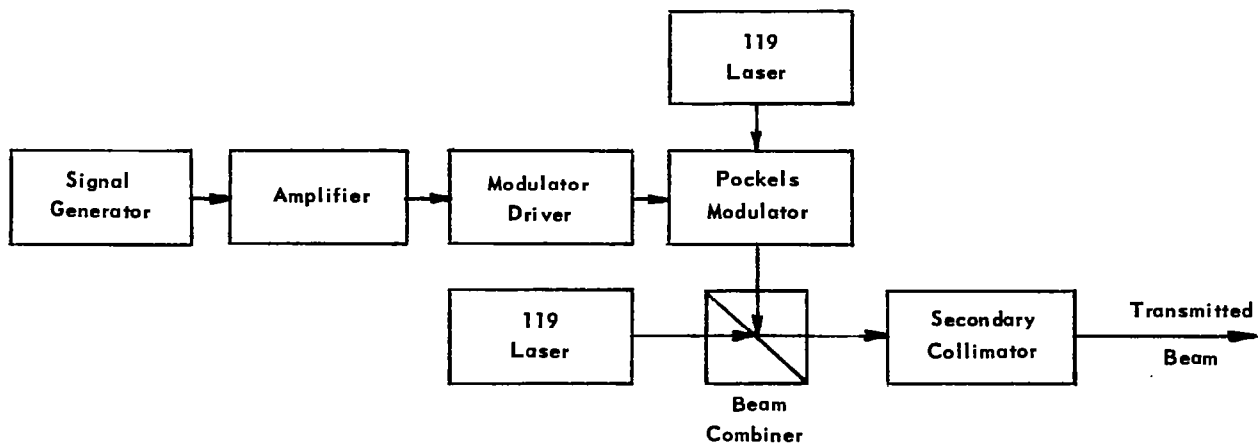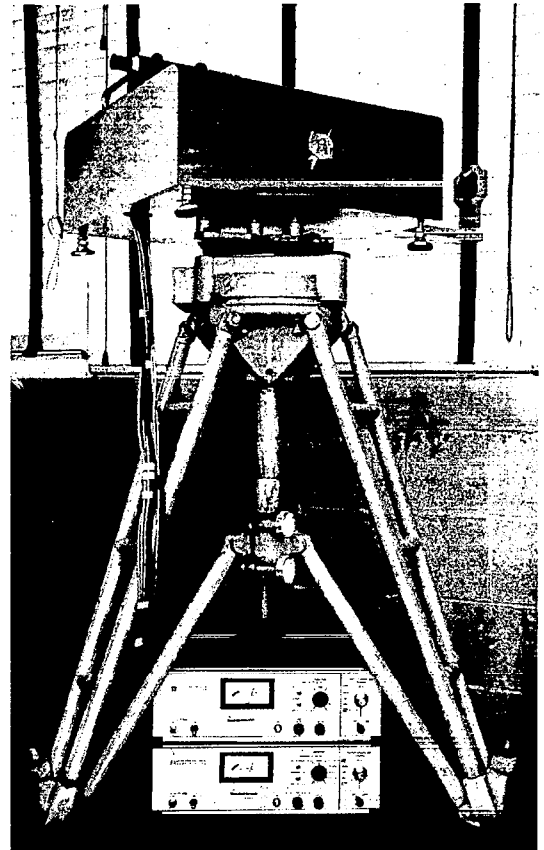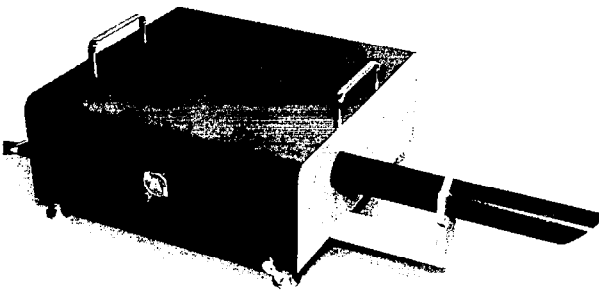
TRANSMITTER

RECEIVER

Figure 26.   TRANSMITTED REFERENCE HETERODYNE LASER
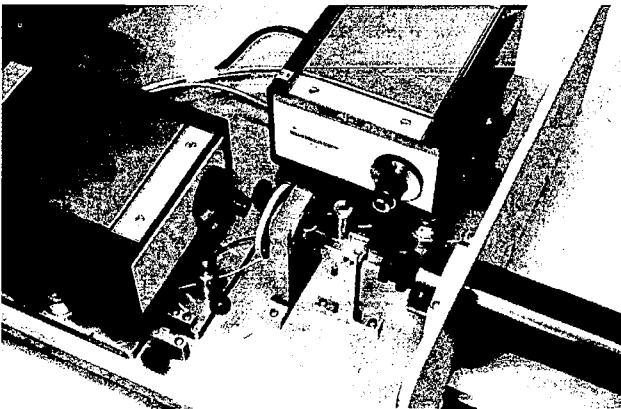COMMUNICATIONS SYSTEM

57

C-Tripod Assembly

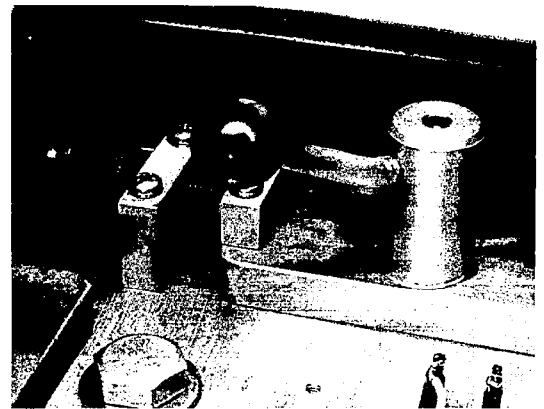B-Transmitter Unit

A-Optical Layout

D-Adjustments

Figure 27.   BREADBOARD MODEL - TRANSMITTER UNIT

58

18 mm. thick aluminum surface plate. This is a strain relieved metal that resists warping and bending. The lasers are mounted to carrier plates on three thumbscrew legs that permit adjustment of laser height and angle of the case with respect to the baseplate. The carrier plates slide on the baseplate surface and are oriented by three thumbscrew adjustments that allow translation of the laser and angular adjustment in the plane of the baseplate. Thumbscrew stops are provided for locking the vertical and horizontal adjustments and, in addition, two hold down clamps are provided on the carrier plate at the front and rear of the case. Figure 27d shows the constructional detail of a horizontal adjuster and the hold down clamp. This method of mounting the lasers provides a versatile arrangement for alignment of the beams with respect to each other and the external optical components. The locks assure that alignment is maintained during normal handling of the transmitter unit. Experience with this mounting arrangement has proven it to be adequate for all adjustment procedures.

Details of the modulator holder are shown previously in figure 15 b. The ADP crystal is wedged between two brass electrodes. A small detent is machined on the back of the electrodes for keying with a spring loaded ball check that is screwed into the plastic half shell. The ball check maintains compression on the crystal through the clamping action of the electrodes. The crystal can be rotated 100 degrees about the optical axis when mounted in the holder. Electrical contact is made to the electrodes on the ends opposite those shown in the picture. Twisted pair leads

are soldered directly to the end surfaces and bent aside to prevent inter-ference with the laser beam.

Beam divergence of the model 119 laser without the colli-mating telescope is 10 milliradians, with the collimating telescope it is less than 0.3 milliradian. Both the signal carrier and local oscillator lasers are used with the integral collimating optics. A secondary colli-mating telescope is provided for spreading the combined output to one milliradian beam divergence. One milliradian gives a one meter spot size at one kilometer. The pointing precision required for a one milli-radian beam divergence is 0.5 millimeter deflection at the end of a meter long lever arm at the transmitter. This gives a shift of one half the beam diameter at the target. The double collimator optics configuration is chosen, so that highly collimated beams traverse the optical paths in the interferometer; thereby minimizing optics lasers in the modulator and insuring precise beam alignment. The secondary beam collimator is a simple Galilean telescope. An exaggerated ray diagram is shown in Figure 28. The parameters are defined as follows: $d_1$ is the diameter of the objective lens, $d_2$ is the diameter of the beam at range $\tau$, $x_1$ is the object distance, and $x_1$ is the image distance. By similar triangles:

$$\frac{\tau + x_1'}{d_2} = \frac{x_1'}{d_1} \tag{102a}$$

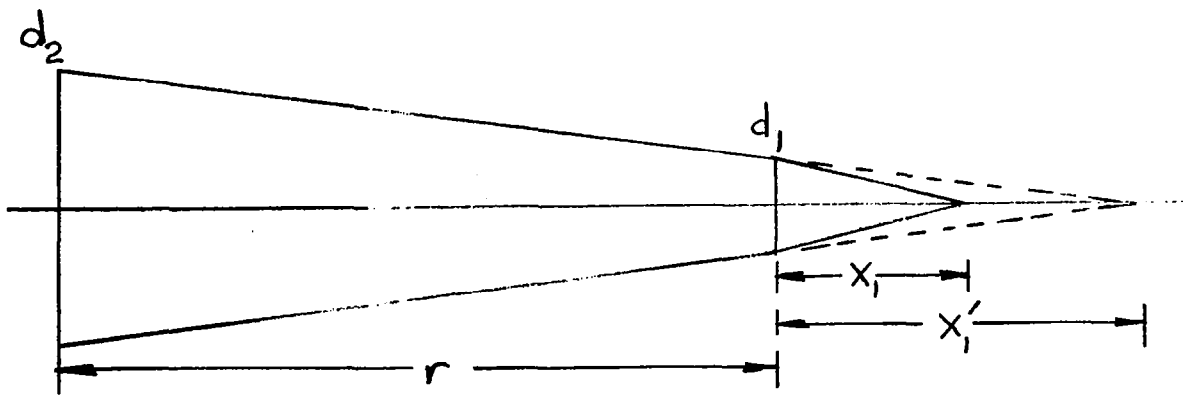therefore:

$$x_1^1 = \frac{r\, d_1}{d_2 - d_1} \tag{102b}$$

Figure 28.   SECONDARY BEAM COLLIMATOR RAY DIAGRAM

From the lens maker's formula:

$$\frac{1}{x_1} + \frac{1}{x_1'} = \frac{1}{f_1} \tag{103a}$$

where $f_1$ is the focal length of the objective lens.  Therefore:

$$x_1' = \frac{f_1 \, x_1}{x_1 - f_1} \tag{103b}$$

Combining (102b) and (103b) and solving for $x_1$:

$$x_1 = \frac{r \, f_1 \, d_1}{r d_1 - f_1 \, (d_2 - d_1)} \tag{104}$$

Substituting design values for the breadboard system:  $r = 10^3 \text{m}$, $f_1 = -0.401 \text{m}$, $d_1 = 0.044 \text{ m}$, $d_2 = 1\text{m}$:  $x_1 = -0.397$ meter.  Spacing between the eyelens and the objective lens is $|\, x_1 |$ plus the focal length of the

eyelens, $f_2$. Let $f_2$ = 0.047 m and:

$$\zeta = | x_1 | + f_2 = 0.444 \text{ m} \tag{105}$$

A fine screw thread is provided on the eyelens mount to permit adjustment of $\zeta$ to the optimum value given by (105).

Alignment of the optical components in the transmitter unit is essential for good spatial mixing of the laser beams. The following alignment procedure is recommended for optimum performance. Adjust each laser collimating lens individually for minimum spot size on a white card at 30 meters with all optical components removed from the transmitter unit, i.e. modulator, beam combiner, and secondary collimator. Install the beam combiner and align the carrier laser beam with respect to the base-plate and the center of the circular exit aperture. Centerline of all optics is 10.2 cm above the baseplate. Align the local oscillator laser to the signal carrier laser by superimposing the L.O. laser beam on the signal laser beam on a white card at 5 and 30 meters respectively. This may be done simultaneously with the right angle combiner. Install the modulator in the signal carrier laser beam path. The crystal is wedge shaped i.e. the end faces are not parallel, so the signal carrier beam will deflect away from the L.O. beam. With the crystal rotated in the holder to operating position, adjust the signal carrier laser to the center of the modulator crystal and superimpose it on the reference beam at 5 and 30 meters. Install the secondary collimator if desired and the system is aligned. Optimum mixing should be observed anywhere
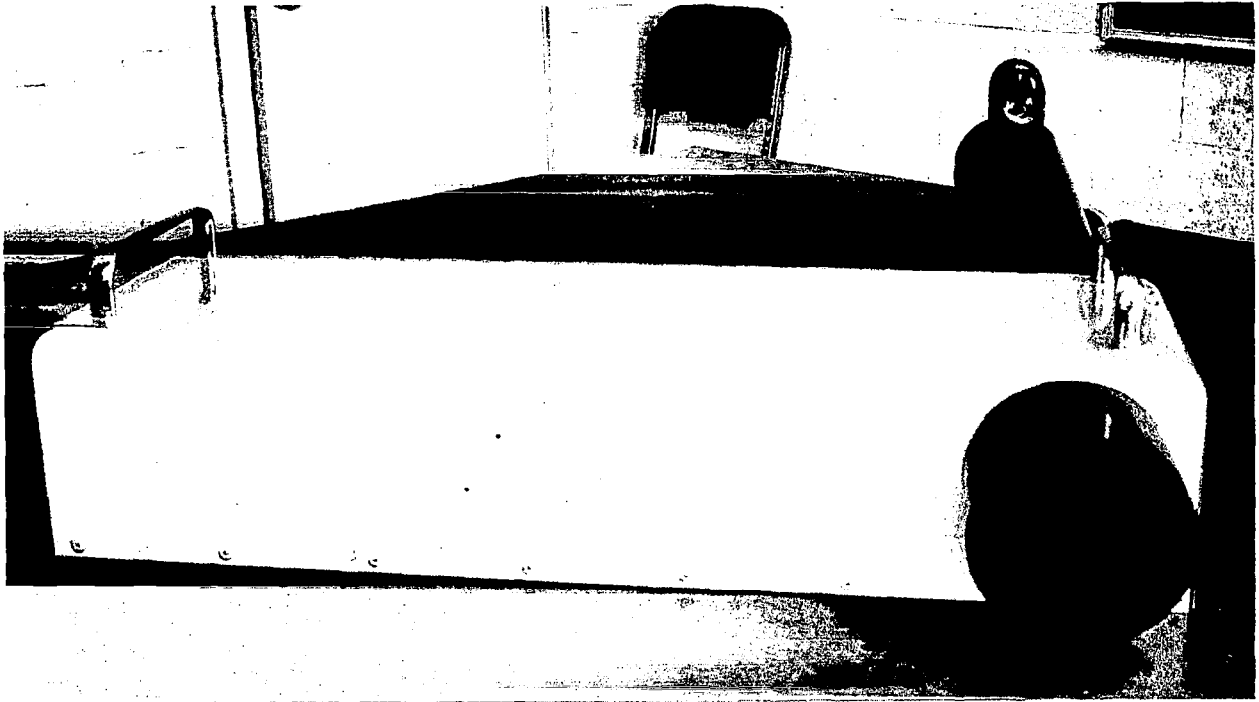
A
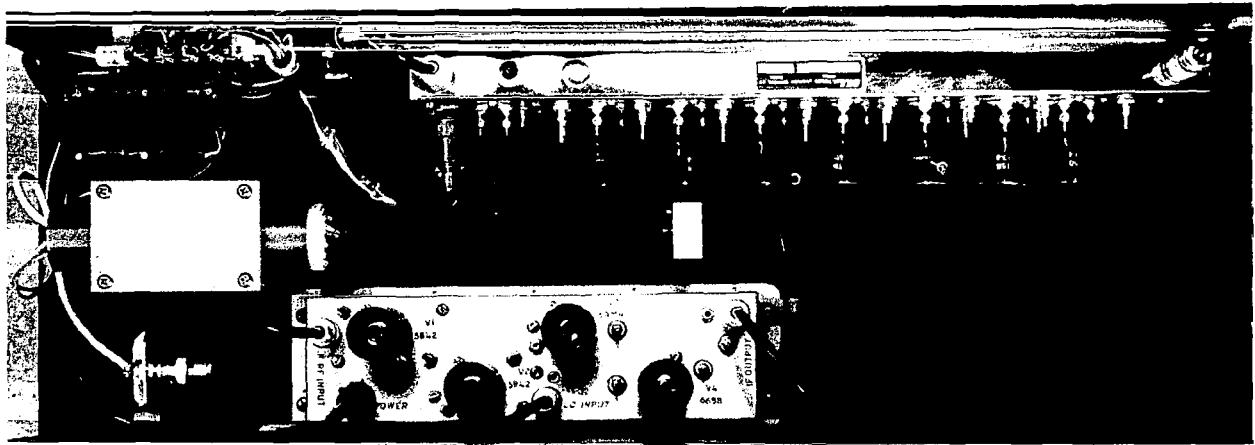


B

Figure 29.   BREADBOARD MODEL - RECEIVER UNIT

in the propagation path of the transmitter unit.

## 2. Receiver Unit

An overall view of the receiver unit is shown in Figure 29A. It consists of a Newtonian telescope, 7X spotting scope, and a receiver box. The telescope primary lens is an f/10, 10.8 cm diameter spherical mirror. It is installed on a conventional three point mounting for ease of alignment. The secondary mirror (mirror diagonal) is mounted on a single, vertical post near the entrance to the tube. Interior details of the receiver box are shown in Figure 29B. It contains a field stop for limiting the field of view of the receiver, the photomultiplier assembly including a narrow band spectral filter, the converter chassis and the IF amplifier chassis containing the limiter, discriminator, and video amplifier.
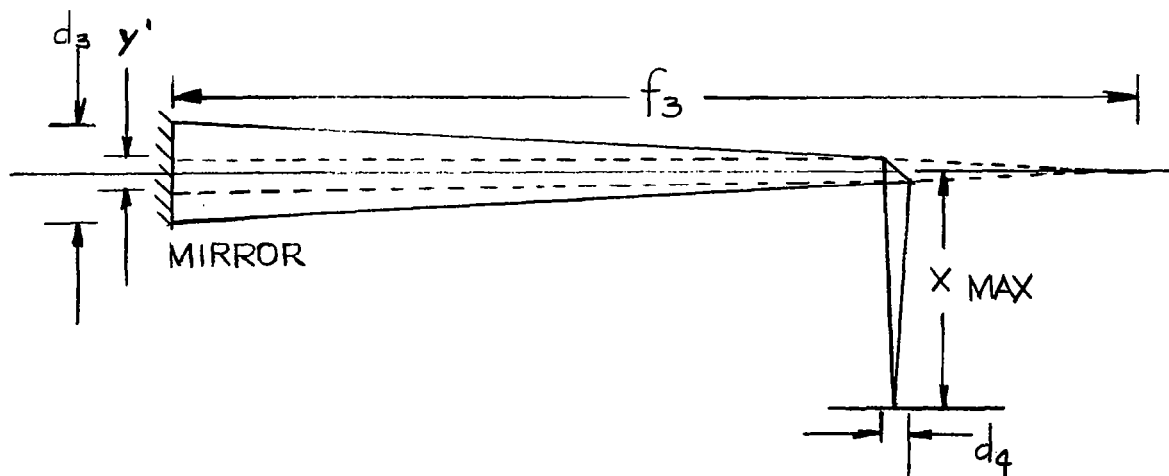
Geometry of the receiver optics is shown in Figure 30.



Figure 30. RECEIVER OPTICS GEOMETRY

The receiver beam angle is given by

$$\theta_{rec} = 2 \tan^{-1} \frac{d_4}{2 f_3} \tag{106}$$

where $d_4$ is the diameter of the circular field stop and $f_3$ is the focal length of the primary mirror. Design value for $\theta_{rec}$ is a milliradian and since $f_3 = 114$ cm.

$$d_4 = \theta_{rec} f_3 = 1.14 \text{ millimeters} \tag{107}$$

An adjustable iris diaphragm is used as the field stop in order to obtain the design beam width as well as larger fields of view. The secondary mirror is an elliptical diagonal of dimensions: 27 mm x 38 mm x 6.4 mm thick. Blockage due to the beam diagonal is given by the projection of the long dimension normal to the incident beam. The projected dimension is given by

$$y' = y \cos (45^o) = 27 \text{ mm.} \tag{108}$$

The effective collecting area of the mirror is given by

$$A_{eff} = \frac{\pi}{4} (d_3^2 - y'^2) = 89.4 \text{ cm}^2 \tag{109}$$

where $d_3$ is the diameter of the primary mirror. The effective diameter is that which gives $A_{eff}$ and is $d_3' = 10.6$ cm. It is apparent that the diagonal blocks very little of the lens aperture. The diagonal may be placed anywhere that it does not vignette the converging beam. By similar triangles the maximum allowable distance from the center of the beam

65

diagonal to the plane of the field stop is given by:

$$X_{max} = \frac{y' \, f_3}{d_3} = 27.9 \text{ cm.} \tag{110}$$

Since the field of view is very narrow, this holds for all beam angles.

The spectral filter used on the photomultiplier is designed to the following specifications: bandpass 2.5 Å, plus 1 Å minus 0, at 6328 Å, plus 1 Å minus 0, transmission 35% minimum, blocked for S-20 response; diameter 2.54 cm. The filter is evaluated by mounting it on a rotatable holder and measuring the transmission characteristics for the 6328 Å HeNe laser line. Maximum transmission is measured to be 56% at an incident beam angle of 2.5 degrees with respect to the normal. The filter is mounted to the photomultiplier holder with a wedge spacer inserted to give a 2.5 degree angle of incidence for the transmitted beam. The transmission measurements are made at room temperature and vary at different temperatures.

The photomultiplier detector is an RCA experimental type C70042CP. It is a ten stage, ruggedized, head-on type tube with S-20 response, curved photocathode, and internally potted dynode bleeder. Current gain at minus 1500 volts anode potential is $4 \times 10^4$, at minus 2000 volts it is $3.3 \times 10^5$. The tube has low distributed anode circuit capacity and small transit time fluctuations for 500 MHz response.

The converter is an LEL model RMP-1-250-70-60-08 receiver module. It consists of an RF preamplifier unit and a converter unit. The RF bandwidth is 70 MHz centered at 250 MHz. The intermediate frequency

is 60 MHz and the IF bandwidth is 8 MHz. Converter gain is > 30 db and noise figure at 250 MHz is 6.3 db. Impedances are 50 ohms. The IF amplifier is an LEL model IMK-1-60-10-50. Center frequency of the IF amplifier is 60 MHz and the 3 db bandwidth is 10 MHz. IF gain is 84 db. The discriminator peak to peak bandwidth is 15 MHz. Video amplifier gain is 23 db. Noise figure of the amplifier is 2.6 db. Impedances are 50 ohms.

### 3. Modulation Demodulation Electronics

The modulator electronics consists basically of a Hewlett-Packard 606 signal generator, a Tektronix 514 video amplifier, and a driver amplifier. A schematic of the driver amplifier is shown in Figure 31. This arrangement permits subcarrier modulation from below 1 MHz to approximately 10 MHz on the light beam. The overall frequency response drops off above 6 MHz. The driver amplifier consists of a cathode follower, buffer input stage to obtain a good impedance match between the pre-driver amplifier and the final. The final driver stage consists of two 4CX250B power tetrodes in parallel operating as a class B amplifier. Gain of the modulator driver is 20 db. Nominal peak to peak voltage input from the 514 amplifier is 50 volts, so the peak swing on the modulator crystal is 500 volts. Interlock relays are installed in the unit, as shown in figure 32, to provide proper sequencing of the tube potentials. The OFF-ON switch applies filament voltage and grid bias to the tubes, activates the air blower, and applies
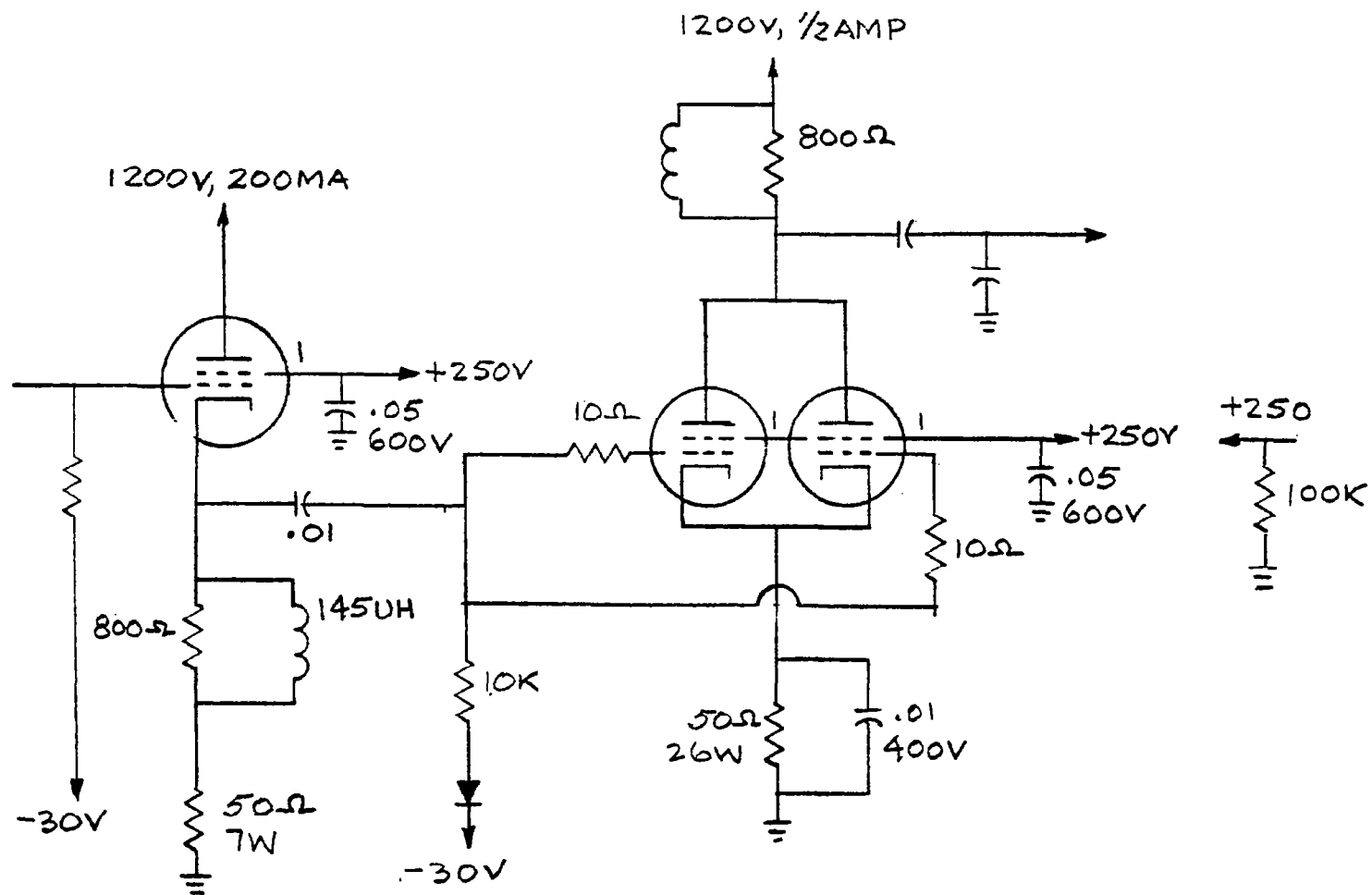
67
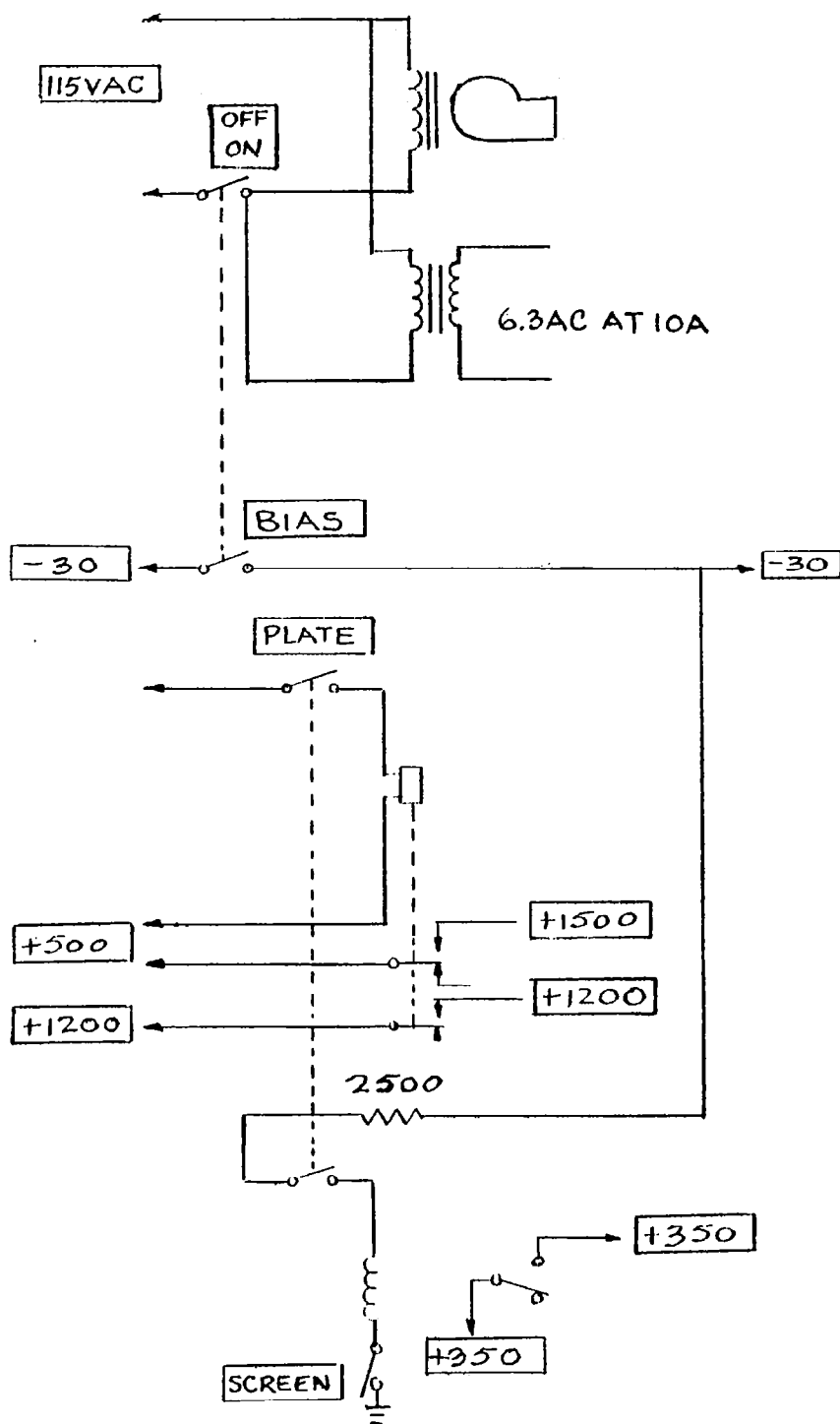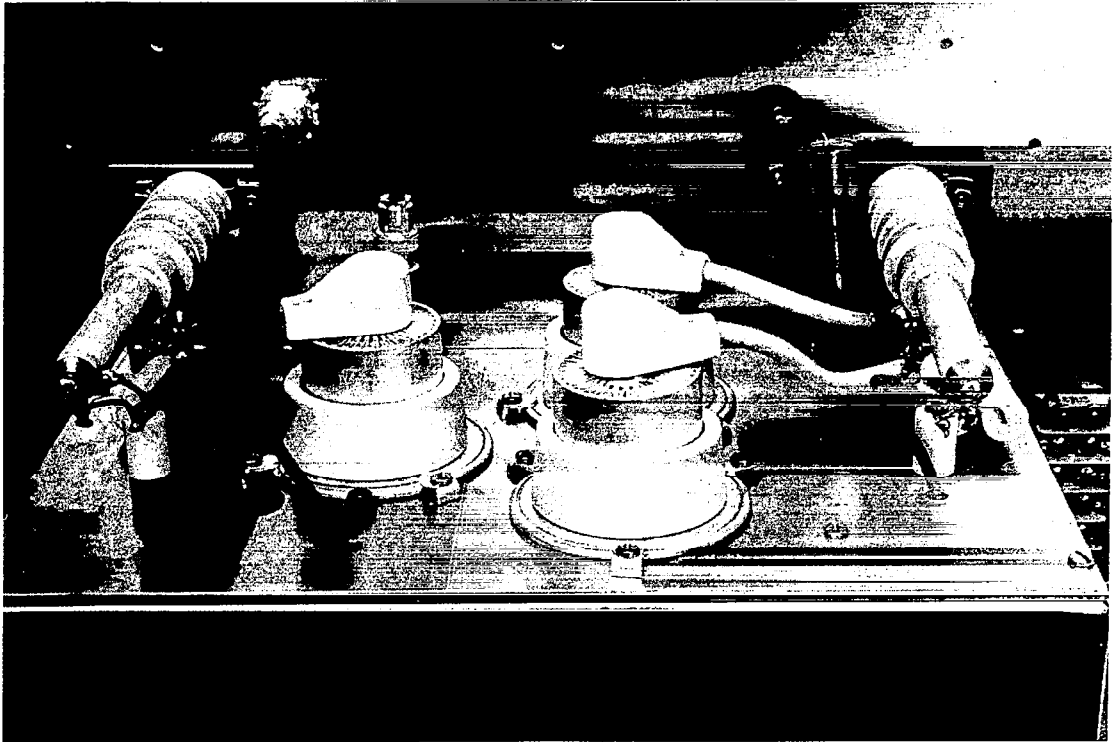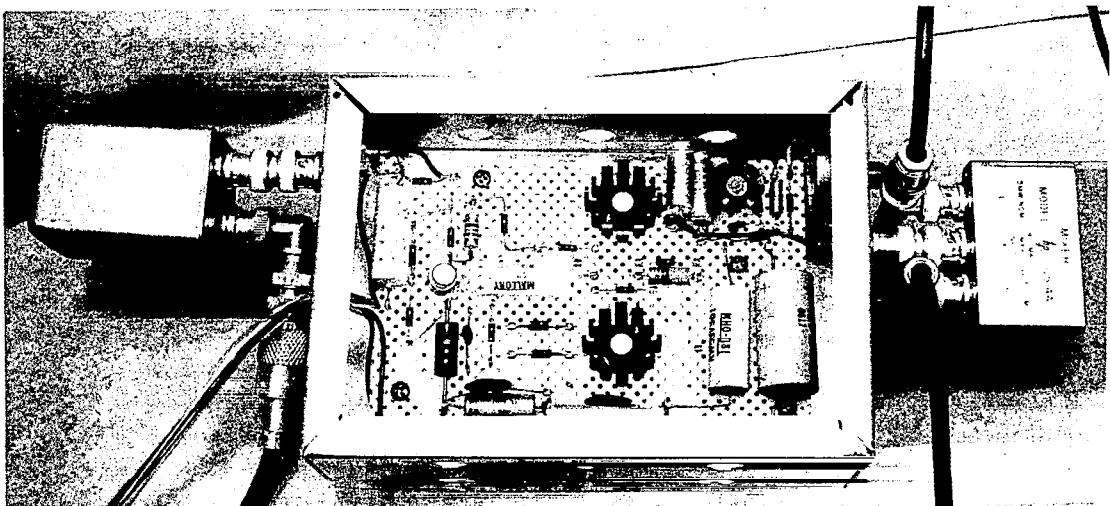
Figure 31.  DRIVER AMPLIFIER SCHEMATIC

Figure 32.   DRIVER AMPLIFIER CONTROLS

A



B

Figure 33.  MODULATION ELECTRONICS

70

voltage to the **screen interlock switch**. The PLATE switch activates the

**plate relay** which **applies** B+ voltages to the chassis. It also closes the

interlock switch in the screen relay circuit. The SCREEN switch applies

voltage to the screen relay, which supplies screen voltage to the tubes.

Associated with each switch on the front panel is a pilot lamp that

indicates the ON position. A photograph of the driver amplifier chassis

is shown in Figure 33A. Power required for the amplifier is:  6 Vac  at

9 amps filament supply, 350 Vdc at 100 ma screen supply, 1000 Vdc at 700

ma plate supply, and -30 Vdc grid bias supply. The filament and plate

relays operate from ac line voltage.

   A block diagram of the modulation system for broadband

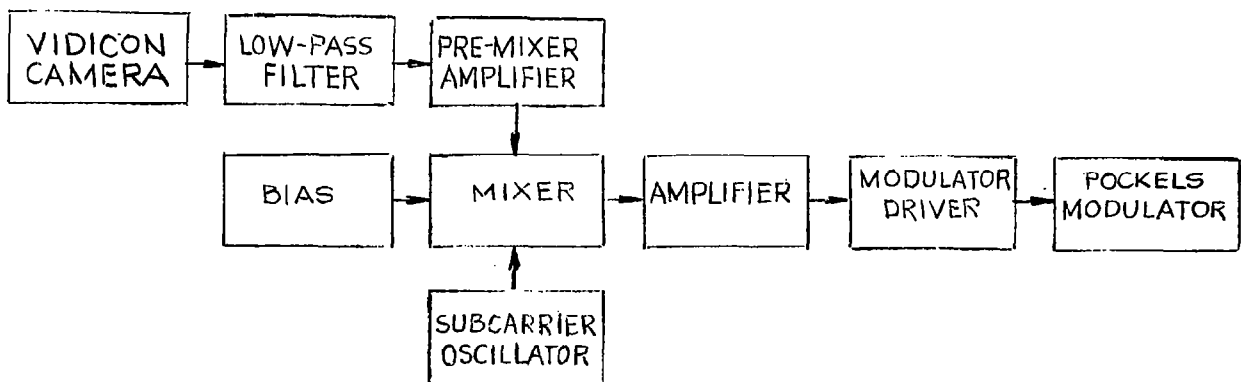video modulation is shown in Figure 34.

Figure 34.  BROADBAND VIDEO MODULATION

The signal source is a 3 MHz bandwidth, vidicon television camera. It is necessary to translate the video signal up in frequency to avoid the laser servo noise spectrum in the detector output. This noise problem is discussed in detail in Section III.C.1. A Hewlett-Packard model 10514A diode bridge mixer is used to amplitude modulate the video signal on the subcarrier. Input impedance of the mixer is 50 ohms and maximum drive current in the X port is 40 ma. An amplifier is required to obtain optimum drive into the mixer. A schematic diagram of the pre-mixer is shown in Figure 35. Figure 33B is a photograph of the chassis showing the input filter and the bridge mixer. Input to the modulator driver in the broadband video mode of operation is nominally 30 volts peak to peak, so the peak drive on the ADP crystal is 300 volts. Voltage swing of the individual video frequency components depends upon the depth of modulation of the video on the subcarrier.

The demodulation electronics follows the FM discriminator and video amplifier of the receiver IF amplifier. The signal at this point, ignoring noise, is simply the subcarrier or in the broadband modulation case, the subcarrier plus sidebands. In the wideband case the detected waveform is first compensated by passing it through a low pass filter. The waveform is then envelope detected. The detected video signal is amplified and applied to a CRT monitor for display purposes.
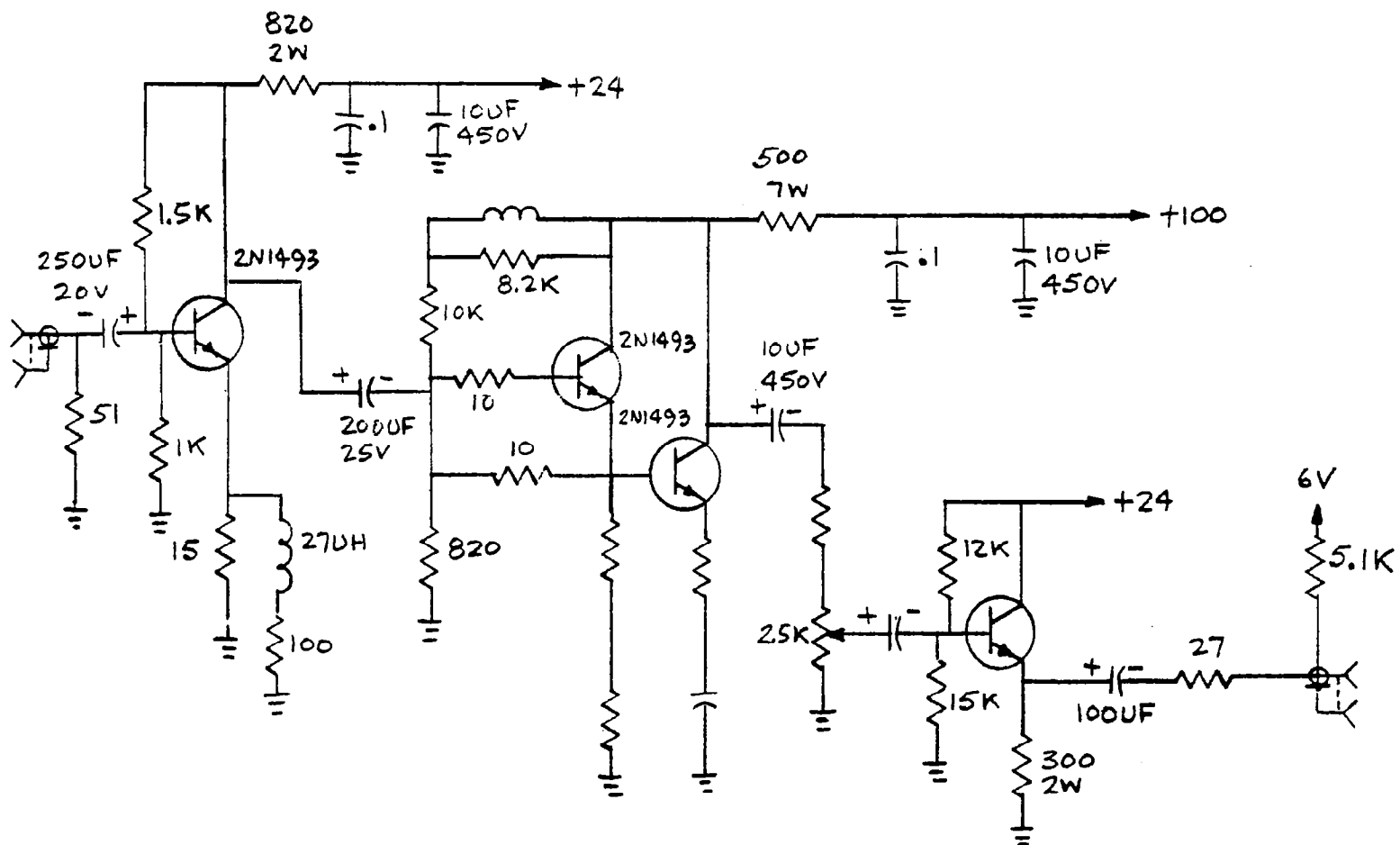
Figure 35.   MIXER PRE-DRIVER AMPLIFIER SCHEMATIC

73

## B. Performance Analysis

### 1. Signal Considerations

Signal power received at the receiver in a one-way link is given by

$$P_{rec}^{rec} = P_m \, e^{-\alpha r} \, \frac{A_{rec}}{A_{trans}} \qquad (111)$$

where $\alpha$ is the atmospheric attenuation factor, $A_{rec}$ is the area of the receiver aperture, and $A_{trans}$ is the area of the transmitted beam in the plane of the receiver. Assume that $\alpha << 1$, and that $A_{trans} > A_{rec}$. Substituting, (111) becomes:

$$P_{rec}^{rec} = \frac{P_m \, d_3'^{\,2}}{r^2 \, \theta_b^2} \qquad (112)$$

where $\theta_b$ is the transmitter beam divergence. The expression does not account for optics losses in either the receiver or the transmitter. Figure 36 shows $P_{rec}^{rec}$ for ranges from 1 to 5 kilometers assuming $d_3' = 10.6$ cm, $P_m = 10^{-4}$ watts, and $\theta_b = 10^{-3}$ radians.

| Range $(r)$ meters | Received Signal Power $(P_{rec}^{rec})$ Watts |
|---|---|
| $10^3$ | $1.12 \times 10^{-6}$ |
| $2 \times 10^3$ | $2.8 \times 10^{-7}$ |
| $3 \times 10^3$ | $1.24 \times 10^{-7}$ |
| $4 \times 10^3$ | $7.01 \times 10^{-8}$ |
| $5 \times 10^3$ | $4.48 \times 10^{-8}$ |

Figure 36. RECEIVED SIGNAL POWER AS A FUNCTION OF RANGE

74

Note that if the secondary collimator is removed, $\theta_b' = 0.3 \times 10^{-3}$ radians, and $P'^{rec}_{rec} = 10\, P^{rec}_{rec}$.

Optics losses in the transmitter are due to the collimator lens elements, the right angle prism beam combiner, and the modulator crystal. Lens element losses are ignored because the laser output is normally measured with the collimator in place. The beam combiner causes a loss of one half of the available laser power or 3 db. A special prism can be used as a beam combiner in an operational system to eliminate this power loss. The modulator loss, since this is a phase modulator is simply the light attenuation through the crystal. This is nominally 3 db. Since the output of the model 119 laser is usually greater than 100 microwatts, the assumption that $P_m = 10^{-4}$ seems valid even considering the transmitter optics losses. As the laser tube ages, of course, $P_m$ reduces proportionately.

The receiver optics losses are due to the reflection loss of the primary and secondary mirrors and the transmission loss of the narrow band filter. These losses are approximately 4 db. It is noted later that receiver losses do not affect performance of background limited systems, since the background noise power is reduced proportionately to the signal power.

The assumption that $\alpha r \approx 1$ is not necessarily valid at relatively long ranges even under good seeing conditions. Watkins[5]

[5] Watkins, M. C. "Study of Laser Application to Velocity Measuring System", AAI Corporation, Report ER-4131, AF 29(600)-4136. Sept. 1965.

reports that one way atmospheric attenuation losses at 0.633 microns are 6 db per kilometer or less, 95% of the time. This worst case number corresponds to an $\alpha = 1.39 \times 10^{-3}$ meter$^{-1}$, or 720 meter air. Since visible range is on the order of several attenuation lengths[6], visibility in this worst case is limited to 2-4 kilometers. In figure 37 the received signal power is given as a function of range assuming 3 kilometer air, $\alpha = 0.3 \times 10^{-3}$ meter$^{-1}$. The signal loss compared to the values in Figure 36 is also given.

| Range (r) Meters | Received Signal Power ($P_{rec}^{rec}$) Watts | Signal Loss db |
|---|---|---|
| $10^3$ | $8.26 \times 10^{-7}$ | -1.3 |
| $2 \times 10^3$ | $1.54 \times 10^{-7}$ | -2.6 |
| $3 \times 10^3$ | $5.05 \times 10^{-8}$ | -3.9 |
| $4 \times 10^3$ | $2.11 \times 10^{-8}$ | -5.2 |
| $5 \times 10^3$ | $9.99 \times 10^{-9}$ | -6.5 |

Figure 37.   RECEIVED SIGNAL POWER FOR 3 KILOMETER AIR

The signal loss in this case is 1.3 db per kilometer and becomes appreciable at the maximum ranges. Visibility under these conditions is approximately 10 kilometers. Conclusion to be drawn from this discussion is that atmospheric attenuation can be a significant factor in signal degradation with range.

[6] Middleton, W.E.K. "Vision Through the Atmosphere"
University of Toronto Press, 1958.

## 2. Noise Considerations

Consider noise in the receiver due to a white noise background of radiance, $I_{rad}$. The received noise power is given by

$$N_o = I_{rad} \; W \; A_{rec} \; \psi \qquad (113)$$

where W is the receiver optical bandwidth and $\psi$ is receiver solid angle. Substituting for $A_{rec}$ and $\psi$, (113) becomes:

$$N_o = \frac{\pi^2}{16} \; d_3'^2 \; \theta_{rec}^2 \; I_{rad} \qquad (114)$$

Data on $I_{rad}$ is tabulated by several sources[7], the values in figure 38 are typical.

| Source | $I_{rad}$ ($\mu$ w/cm$^2$/ $\mu$ / sr) |
|---|---|
| Direct Sunlight | $3 \times 10^9$ |
| Sunlight Cloud | $2 \times 10^4$ |
| Sunlight Earth | $1.5 \times 10^4$ |
| Day Sky | $2 \times 10^3$ |
| Direct Moonlight | $4 \times 10^2$ |

Figure 38.   RADIANCE AT 0.633 MICRONS FOR SELECTED SOURCES

[7] LaRocca  "Fundamentals of Infrared Technology"
University of Michigan, 1964

As a worst case example, consider the breadboard system working against a sunlit earth background: $N_o' = 2.68 \times 10^{-10}$ watts. The additive background noise is attenuated by the receiver optics losses, so the signal-to-noise ratio may be calculated using the numbers in Figure 36, assuming no atmospheric attenuation. At 5 kilometers for example:

$$\left(\frac{S}{N}\right)_{background} = \frac{P_{rec}^{rec}}{N_o'} = 1.67 \times 10^2 = 22 \text{ db.}$$

This becomes 15.5 db for 3 kilometer air. It is apparent that the breadboard system is not background noise limited.

Performance of the photomultiplier involves three sources of noise: noise due to the dark emission current of the photocathode, noise due to the average signal photocurrent, and thermal noise generated in the load resistance. The expression for the ratio of signal current to tube dark current is[8]

$$\left(\frac{S}{N}\right)_{i_d} = \frac{i_k}{\left[2e\, i_d\, (1 + \frac{G}{m-1} B)\right]^{1/2}} \tag{115}$$

where $\quad$ $i_k$ is the average signal cathode photo current

$\quad$ e is the electronic charge, $1.6 \times 10^{-19}$ coulombs.

$\quad$ $i_d$ is the tube dark current

$\quad$ m is the secondary emission ratio per stage, $\approx 4$

$\quad$ G is a statistical factor = 1.54

$\quad$ B is the receiver bandwidth

[8] "Phototubes and Photocells" RCA Technical Manual PT-60, Lancaster, Pa. 1963, pp. 55 ff.

The expression for the ratio of signal current to noise in signal current (shot noise) is similar with $i_d$ replaced by $i_k$. Therefore:

$$\left(\frac{S}{N}\right)_{i_k} = \left[\frac{i_k}{2\ e\left(1 + \frac{G}{m-1}\right) B}\right]^{1/2} \tag{116}$$

Note that the signal to the shot noise ratio varies directly as the square root of the average signal current whereas the signal to dark current ratio is proportional to the average signal current directly. For $i_k > i_d$ , $\left(\frac{S}{N}\right) i_k$ is the smaller quantity. In the experimental model this condition applies and shot noise is the predominant noise source. For the optimum value of tube load resistance, the rms Johnson noise voltage is equal to the dark current noise voltage. Therefore thermal noise may be ignored with respect to shot noise also.

The average photocathode signal current is

$$i_k = P_{rec}^{rec} \quad T \quad \beta \tag{117}$$

where T is the transmission factor of the receiver optics and $\beta$ is the cathode sensitivity. The S-20 photocathode has a radiant sensitivitiy of $2.3 \times 10^{-2}$ amp/watt at 0.633 microns. Bandwidth of the RMP-1 converter input stage is 70 MHz. From an earlier discussion T = 0.4 $\left(\frac{S}{N}\right)_{i_k}$ is given in Figure 39 for several ranges using values of $P_{rec}^{rec}$ from Figure 36. This is the signal to noise ratio at the optical detector.

| Range Meters | $(\frac{S}{N})_{i_k}$ (db) |
|---|---|
| $10^3$ | 12.4 |
| $2 \times 10^3$ | 9.4 |
| $3 \times 10^3$ | 7.6 |
| $4 \times 10^3$ | 6.4 |
| $5 \times 10^3$ | 5.4 |

Figure 39.   DETECTOR NOISE LIMITED S/N AS A FUNCTION OF RANGE

These S/N ratios are considerably smaller than the worst case background (S/N) = 22 db; demonstrating that the breadboard system is detector noise limited.

C.  Experimental Data

1.  Servo Noise

The Model 119 lasers are locked to the Lamb dip region of the mode pattern by a servo system.  A 5 KHz modulation is applied to the piezoelectric mirror mount that causes amplitude modulation of the laser output depending upon the shape of the mode pattern at the operating point.  This AM'ing of the beam is detected by a photocell, amplified and compared in a phase comparator with the modulating wave-form.  An error signal is generated and applied to the mirror to correct for mirror drift.

A noise spectrum is generated in the receiver output of the breadboard model due to the servo noise. The mirror motion causes FM'ing of the beam as well as the amplitude modulation. The differnce frequency contains the beat of the two servo noise spectra. There are line spectra at 5, 10 and 15 KHz. The noise spectrum peaks below 1 KHz. This noise prevents use of baseband modulation with the lasers in the servo lock position. Experience has shown that after 4 to 6 hours operation the lasers stabilize and servo lock operation is not required to keep the difference frequency within the bandpass of the receiver.

2. Subcarrier Modulation

The system was operated over a 300 meter link to demonstrate qualitatively system performance. Subcarrier modulation at 2-4 MHz is detected with excellent signal to noise when the lasers are stabilized. Narrow band filters are used to reduce receiver bandwidth. Drive voltage on the modulator crystal is nominally 150 volts. No quantitative measurements of system performance were made during this phase of the contract.

3. Video Modulation

In the case of video modulation signal quality is very poor. Frequency stability of the laser beat was not adequate for optimum tuning of the receiver in the unlocked servo condition. In the servo lock condition the noise spreads the difference frequency spectrum over 20 MHz at a low frequency rate so that signal is lost at

the fixed tuned receiver. Performance will be measurably improved by reducing servo noise and incorporating a tracking local oscillator in the receiver. These improvements will permit quantitative evaluation of breadboard model performance.